THESIS FOR THE DEGREE OF DOCTOR OF PHILOSOPHY IN APPLIED CHEMISTRY

Nanoparticle Self-assembly on Prefabricated Nano Structures.

JOHNAS EKLÖF-ÖSTERBERG

CHALMERS

Department of Chemistry and Chemical Engineering

Division of Applied Chemistry

CHALMERS UNIVERSITY OF TECHNOLOGY

Göteborg, Sweden 2018

Nanoparticle Self-assembly on Prefabricated Nano Structures.
JOHNAS EKLÖF-ÖSTERBERG
ISBN 978-91-7597-819-2

Doktorsavhandlingar vid Chalmers tekniska högskola
Ny serie nr. 4500
ISSN 0346-718X
Department of Chemistry and Chemical Engineering
Division of Applied Chemistry
Chalmers University of Technology
SE-412 96 Göteborg
Sweden
Telephone: +46 (0)31-772 1000

Cover:
A schematic figure introducing the idea of molecular based electronics. Subsequently a SEM micrograph over a nanoparticle dimer linked with benzene 1,4-dithiol.

Chalmers Reproservice
Göteborg, Sweden 2018

Nanoparticle Self-assembly on Prefabricated Nano Structures.
JOHNAS EKLÖF-ÖSTERBERG
Department of Chemistry and Chemical Engineering
Division of Applied Chemistry
Chalmers University of Technology

Abstract

The demand for more powerful computers have been increasing ever since the first semiconducting devices were invented in the second half of the 20^{th} century. The demand for an increase in computing power have escalated since the start of modern computer technology, however conventional techniques are reaching the limits regarding the downscaling of semiconducting based logic circuits. One way of circumventing these challenges is to utilize molecules in integrated circuits instead of conventional semiconducting designs. Molecules can be synthesised in molar amount and can act as rectifiers, transistors, switches and conducting wires. They are also a factor ten smaller than the node size of commercial available transistors. However a method for integrating single molecule into an electronic grid in order to construct molecular based logic circuits is not known today. Scientists have at this point been able to contact and measure on molecules, using techniques such as the break-junction method, however it has been difficult to contact single molecules in parallel, which is needed in order to compete with conventional semiconducting industry.

This thesis focus on contacting single molecules by isolating them between nanoparticles (or dimers), that can be guided onto prefabricated structures in an approach that utilizes both top-down and bottom up concepts. The deposition efficiency was tested on a variety of materials, including metals and functionalized surfaces. This was done as a pre-study in order to determine the optimum conditions for particle deposition. A model based on a combination of DLVO-theory (Derjaguin, Landau, Verwey and Overbeek) and RSA (random sequential adsorption) was developed in order to explain the deposition process and the interactions between particles and a substrate. Spatial descriptive statistics were used to see if the pattern of the particles from simulated and real depositions deviated from CSR (complete spatial randomness) and to compare the inter-particle distances. Potential measurements were compared to the nanoparticle densities. The experiment showed that materials such as nickel and aluminium attract the negatively charged particles used in this thesis. As a next step, particles were deposited on arrays of nanosized objects of different shape and size in order to optimize deposition parameters and electrode design. Finally, electrical measurements of BDT (benzene-1,4-dithiol) and HDT (1,6-hexanedithiol) linked dimers were performed as a proof of principal, indicating that conductance through BDT is higher compared to HDT. More experiments is needed in order to confirm this. However, the deposition is still inefficient, only 5 % of the nanogaps are filled with a dimer. This number needs to be increased in order for molecular electronics to be able to compete with upcoming techniques such as extreme UV-lithography.

Keywords: Self-assembly, Nanoparticles, single molecular electronics, Nanofabrication

Acknowledgements

I would first of all acknowledge ERC for funding my research here at Chalmers through the ERC StG SIMONE. Subsequently I want to acknowledge Myfab National Access program (at MC2 Nano Fabrication Laboratory, Chalmers) for funding my start at MC2. Furthermore, I want to send my gratitude to Kasper, my main supervisor for being supportive throughout my PhD studies and for spending all the extra time and effort into helping me with both research and life in general. I know now the difficulties of fulfilling a PhD, however I cannot imagine the difficulties of supervising several PhD students at once. I would also like to thank Samuel, my co-supervisor for teaching me everything worth knowing regarding clean room techniques, but also for always helping me discussing questions regarding production or results, 24/7. I would also like to thank the nano-group for all the nice discussions and feedback during the years. I would specially like to thank Tina and Behabitu for helping me with all my questions regarding molecules and synthesis of molecules and molecule linked dimers. Also thanks Behabitu for drawing all the molecules for me in Chemdraw. Thanks Victor for all nice MATLAB and LATEX discussions. I also want to say thanks to Kaspers group, both previous and present members for making such a great working environment, it is always possible to ask anyone for help, regardless the subject. Thanks Ambra and Mikaela for being such fun office mates and for making every day something special at work. Thanks Lotta for keeping our floor together, for all the candy and for reminding me to let in some oxygen into my office. Subsequently I want to acknowledge the staff and infrastructure at MC2, for learning me all the machines you have helped with and for all good advices regarding micro and nanofabrication. A special thank to Ulf Södervall for helping me setting up my project at MC2. A great thank to Astghik and Kyung for the clean room support. Thanks to Mattias and David for helping me escape the reality with a glass of beer, or two, especially during the fire alarms. I would also like to thank the entire floor eight for creating the lunches and fika's into awesome discussions about nothing and everything.

Thanks to my parents, I love you both. Thank you mamma, Marita for always listening and believing in me. We are both truly humble. Thank you pappa, Roland for all the warmth and joy you have given me and for guiding me through life and for learning me how to chop up a pig and turn it into Chorizo. Thanks to my sister, Sandra and brother, Nichlas for always being there for me. Finally an extremely big thanks to my wife Carin, my bright star in life, for making me laugh and for always supporting me through all the difficulties in life and for always understanding me, even though I do not understand my self, and thanks for giving me Folke, I love you both, more than words can describe.

Johnas

Nomenclature

APTES	(3-Aminopropyl)triethoxysilane
AFM	Atomic Force Microscope
CSR	Complete Spatial Randomness
CTAB	Cetyltrimethylammonium bromide
EBL	Electron Beam Lithography
IEP	Isoelectric Point
IPA	2-propanol
MOSFET	Metal Oxide Semiconductor
NIL	Nano Imprint Lithography
NP	Nanoparticle
PLL-HBr	Poly-L-Lysine Hydrobromide
PMMA	Poly(Methyl Methacrylate)
PZC	Point of Zero Charge
PSD	Percentage of Successful Depositions
SAM	Self Assembled Monolayer
SEM	Scanning Electron Microscope
TEM	Transmission Electron Microscope
UV	Ultra Violet
XEDS	X-ray Energy Dispersive Spectroscopy

Thesis

This thesis consists of an extended summary and the following appended papers:

Paper I **Controlling deposition of nanoparticles by tuning surface charge of SiO_2 by surface modifications**, Eklöf, J., Gschneidtner, T., Lara-Avila, S., Nygård, K. and Moth-Poulsen K., *RSC Advances*, 2016, **6**, 104246-104253.

Paper II **Guided selective deposition of nanoparticles by tuning of the surface potential.**, Eklöf, J., Stolas, A., Herzberg, M., Pekkari, A., Tebikachew, B., Gschneidtner, T., Lara-Avila, S., Hassenkam, T. and Moth-Poulsen K., *EPL*, 2017, **119**, 18004.

Paper III **Parallel fabrication of self-assembled nanogaps for molecular electronic devices.**, Eklöf-Österberg, J., Gschneidtner, T., Tebikachew, B., Lara-Avila, S., and Moth-Poulsen K., *small*, 2018, **0**, 1803471.

Paper IV **Optimazation of geometrical structures designed for assembly of nano-sized objects.**, Eklöf-Österberg, J., Löfgren, J., Erhart, P. and Moth-Poulsen K., manuscript, 2018.

The author has published the following papers which are not included in the thesis.

Paper A **One-pot synthesis of TBTA-functionalized coordinating polymers**, Movahedi, A., Moth-Poulsen, K., Eklöf, J., Nydén, M. and Kann, N., *React. Funct. Polym.*, 2014, **82**, 1-8.

Paper B **Apparent power law scaling of variable range hopping conduction in carbonized polymer nanofibers.** Kim, K. H., Lara-Avila, S., Kang, H., He, H., K., Eklöf, J., Hong S. J., Park, M., Moth-Poulsen, K., Matsushita, S., Akagi, K., Kubatkin S., and Park, Y. W., *Sci. Rep.*, 2016, **6**, 37783.

Paper C **Probing variable range hopping lengths by magneto conductance in carbonized polymer nanofibers.** Kim, K. H., Lara-Avila, S., He, H., Kang, H., Hong, S., J., Park, M., Eklöf, J., Moth-Poulsen, K., Matsushita, S., Akagi, K., Kubatkin, S., and Park, Y. W., *Sci. Rep.*, 2018, **8**, 1-7.

Paper D **Reconfigurable carbon nanotube multiplexed sensing devices.** Xu, X., Clément P., Eklöf-Österberg, J., Kelley-Loughnane, N., Moth-Poulsen, K., Chávez, J. L., Palma, M., *Nano lett.*, 2018, **7**, 4130-4135.

Contribution Report

Paper I	Developed the details of the experimental set-up, functionalized the surfaces. Performed the deposition of nanoparticles, all SEM and KPFM measurements. Developed the ERSA model, and performed the inter-particle distances measurements. Wrote the paper.
Paper II	Designed and produced samples, performed the deposition of particles. Have performed SEM and helped with the AFM measurements. Have written larger parts of the text.
Paper III	Wrote the major part of the text, prepared the nano-electrode samples and performed the deposition of nanoparticles and nanoparticle dimers. Took all SEM micrographs and performed the electrical measurements.
Paper IV	Wrote the text together with Joakim Löfgren, fabricated all nanofeatures, deposited the nanoparticles, took all images using the SEM and analyzed the deposition outcome. Were involved in calculating the correct debye lengths for the theoretical part of the paper.
Paper A	Performed SEM and XEDS measurements.
Paper B	Performed SEM measurements.
Paper C	Assisted in the AFM measurements.
Paper D	Made the electrode samples.
By others	The AFM measurements in paper II plus the force curve fits was performed at the University of Copenhagen by Mikkel Herzberg. The dimer synthesis and the TEM measurements in paper III was performed by Tina Gschneidtner. The DLVO theory and simulations in paper IV was performed by Joakim Löfgren.

Contents

1 Introduction

The time period between the invention of glasses[1] in the 13th century to one of the first computing machines, the punched card tabulating machine[2] in the 18th century is almost ten times shorter compared to the period between one of the first documented wheels,[3] 3500 BCE and glasses. The trend of fast progress continues when looking at the first digital computer ENIAC (1940s)[4] (based on vacuum tubes[5]) and the first semiconducting transistor in the mid 1950s[6], which reduced the cost and volume of the computers in the 60s and 70s.[7,8]

The miniaturization of the components in integrated circuits opened up new possibilities for people to install computers in their homes in the end of the 80s. By the mid 90s, 16 million devices were connected to the internet,[9] this number had increased to more than 3.5 billion devices in year 2016[10] thanks to processors containing smaller electronics components in tighter space. Today, conventional processors uses transistors as small as 14 nm.[11] The trend of downscaling of integrated circuits must continue in order to meet future demands on costs and processing power as 75 billion devices are predicted to be in use in year 2025.[12] However, scientists believe that the conventional downscaling of electronic components will soon reach its limit.[13] It is therefore important to find alternative ways of downscaling electronic components in order to continue the accelerating rate of progress.

Photolithography is the leading technique in semiconductor industry of today.[14,15] Nanofeatures are produced by exposing a resist-coated semiconducting wafer with ultraviolet (UV) radiation through a photo-mask. Parts of the non-exposed resist is dissolved (positive mask) in a developing agent and a pattern is produced.[16] The advantages of photolithography is its ability to produce several components in parallel.[16] Diffraction is the main limit in downscaling[17] which is proportional to the wavelength of the UV-light source.[18] A light source of 193 nm can produce structures with a node size of 14 nm,[17] which is the size of commercially available transistors.[19]

Ways to circumvent the limits of photolithography have been presented during the years, including the mask-less electron beam lithography (EBL), where a focused electron beam writes directly in the resist. The main advantage here is flexibility and the ability to construct features in the sub 10-nm regime.[20] EBL is however not an option for industry due to the low throughput. Other options regarding nanofabrication is nanoimprint lithography (NIL), where a pattern is transferred from a mold which is pressed onto a resist. The advantage with NIL is the ability to produce several features in parallel. Problems with throughput and defects are some reasons why it is not used in semiconductor industry.[21] Extreme UV lithography[22] is perhaps one of the most promising near future nanofabrication techniques, where it will be possible to construct sub-10 nm features in parallel, using a light source with a wavelength of 13.5 nm. The main issue so far has included power supply for the light source and the photomask.[23] The semiconductor industry continues to push the limit of downscaling the size of conventional semiconductor

based integrated circuits, it is however important to continue the research within the field of miniaturization so that the demands on processing power can be met by industry.

One option to conventional semiconductor components could be molecules. Typical molecules for this purpose can be a factor of ten smaller in length than the present node size of any transistor and much smaller by volume.[24] It is also possible to synthesize molar amounts of molecules without any advanced cleanroom techniques.[24] It has been shown during recent years that molecules can function as e.g. conducting wires,[25,26] switches,[27–30] and diodes.[31–34] It is difficult to construct a logic circuit from molecules directly in a solution and it is therefore necessary to connect them onto a grid of electrodes before any electrical measurement can be carried out. Different ways of contacting and measuring single molecules exists today, such as scanning break junction and mechanical break junction.[33,35–42] These techniques are good at investigating conductance of molecules, however they do not possess the ability to measure several molecules in parallel, hence building more advanced circuits. Methods for parallel fabrication of molecularly sized nanogaps are being developed, but due to the width of the devices, they do not discriminate between a single or several molecules in each nanogap. An option could instead be to assemble the molecules onto the electrodes by them-selves. One way of isolating single molecules and measuring them have been presented by Bar-Joseph et al.[43,44] where molecules are attached to two metal NPs (nanoparticles) forming a dimer, this was in turn attached to electrodes via electrostatic trapping. Only one dimer at a time was presented to be captured in this example, however this procedure could in principle be used to isolate several single molecule devices in parallel.

This thesis will focus on the self-assembly of NPs and NP dimers linked with functional molecules onto specific locations on a substrate. Chapter 1 will give the reader background information regarding molecules that can be used for electronics and how to measure them. Chapter 2 will treat the versatility of NPs and how one could synthesis them. A summary of the work published in paper I-IV and some additional experiments, results and discussions will be presented in chapter 2 and 3. The thesis will be given a wider perspective in chapter 4, where the conclusion and outlook will be presented. A more detailed description about the different tools and techniques used in this thesis will be given in chapter 5.

1.1 Molecules for electronics

It was in the mid 70s that scientists proposed that single molecules could be used as electronic components.[31] One of the first electrical measurements on single molecules were presented in 1996, in this case, an STM (scanning tunnelling microscope) tip was scanned over a (111) gold substrate covered by a self-assembled monolayer (SAM) of n-dodecanethiol containing a small percentage of 4,4'-di(phenylene-ethylene)-benzothiolacetate used as a molecular wire (MW) within the SAM. The conductance would then increase when the STM tip scanned over one of the MWs.[45] Alternative methods for measuring a molecule have since then been presented by scientists including the mechanical break

junction.[33,35–38] A nanogap can also be produced in a controlled way by bending a conducting wire placed on a flexible substrate, the wire will thus break and the size of the nanogap will increase as the bending continues, fig. 1.1 a. Another option is the STM-break junction, fig. 1.1 b. The nanogap is here created when a metal tip is crashed into a metal surface covered with the molecules of interest. A nanogap will appear when retracting the tip, giving space for a molecule to attach.[39–42] The two examples seen in fig. 1.1 are good when it comes to examine the conductive properties of a certain type of molecule due to the tunable gap length and the statistic weight of the results. However, it is not possible to fabricate two or more junctions (contact-molecule-contact) in parallel using these techniques and they are therefore not suitable when constructing more advanced logic circuits.

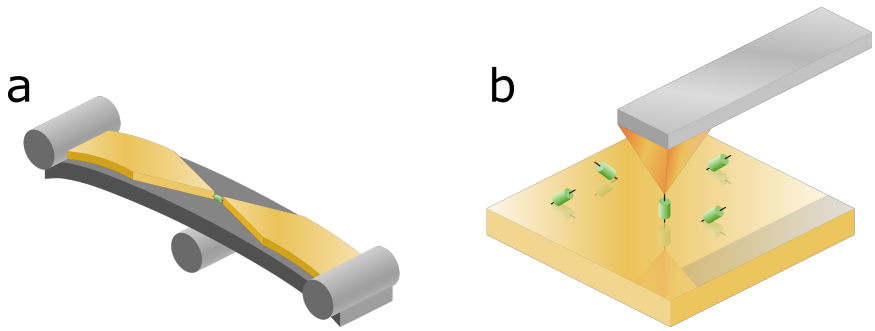

Figure 1.1: *Two examples of break junctions for single molecular measurements. a) A mechanical break junction and b) a scanning tunneling microscopy (STM) based break junction. The green cylinder represents the molecule of interest.*

Other ways of constructing nanogaps suitable for molecular measurements include electromigration breakdown,[46–49] surfactant assisted parallel electroless plating[50] or shadow mask evaporation.[51,52] The challenge in these techniques is to produce gaps in parallel and to capture single molecules in parallel. Research have progressed since the first suggestions on how to electrically measure a molecule and new methods for production of nanogaps have been suggested such as self-assembled nanocrystals used as a mask before evaporating metal electrodes,[53] or the growth of gold nanorods from seed crystals aligned via PMMA channels.[54] Other methods include decreasing nanogaps by the growth of electrodes protected with a SAM to avoid closing the gaps,[55] crack-defined nanogaps[56] and graphene based electrodes,[57] which are all good candidates for how to fabricate nanogaps for molecular electronics. However, one must position billions of molecules in parallel in order to compete with conventional semiconductor industry, which might be a serious issue in relation to the current state of the art.

An interesting alternative approach of depositing several single molecules into defined nanogaps could be to combine molecules with nanoparticles, into larger complexes (so called proto-devices), all in solution and then in turn depositing them onto prefabricated electrodes.[43,44,58–64]

1.2 Molecules suggested for molecular electronics

Several types of molecules with different properties have been suggested for molecular electronics. A molecular wire is designed to conduct in both directions. There are several examples of molecular wires with varying ability to conduct current such as the conjugated benzene 1,4-dithiol,[25] see fig. 1.2 a, 1,4-benzenedimethanethiol[25] and oligophenylethylene.[26] Non-conjugated systems such as 1,6-hexanedithiol[65] does not conduct as well as the conjugated systems and could be used as molecular insulators.[66] Molecules can also act as diodes, much like the semiconducting pn-junctions.[67]

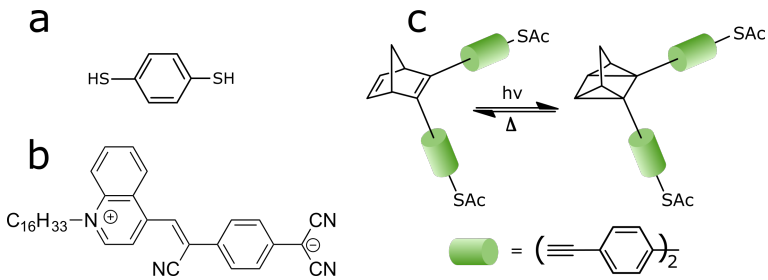

Figure 1.2: *Skeletal formulas of three different molecules, suggested to work in molecular electronics. a) 1,4-benzenedithiol can act as a molecular wire. b) γ-hexadecylquinolinium tricyanoquinomethanide can act as a diode and c) norbornadiene-based photoswitch with embedded oligo(phenylene ethynylene) arms capped with thioacetate groups, able to switch between a conducting nornbornadiene form to a less conducting quadricyclane form when exposing it to light.*

A rectifying molecule is usually asymmetric with an electron donor and acceptor on each side,[66] and asymmetric current-voltage (I-V) was shown by Geddas et al. in 1990 and 1992.[68,69] Other rectifying examples, such as γ-hexadecylquinolinium tricyanoquinomethanide was measured by Metzger in 1999,[70] (see fig. 1.2 b.) using the Langmuir-Blodgett method. There are also examples of switching molecules that can toggle between a conducting and a less conducting state by some external stimuli such as light,[30] heat,[28] mechanical stress[27] and redox[29] to name a few. Light or photo-switches are already applied in molecular thermal storage applications.[71] Tebikachew et al.[24] presents a photoswitch able to switch from a conducting norbornadiene form to a less conducting quadricyclane form when exposing it to light, see fig. 1.2 c.

The majority of the potential difference should be located on the actual molecule and not in the connection between the molecule and any electrode. It is therefore common to attach functional groups to the molecules in order to have sufficient coupling between molecule and electrode. Examples of typical functional groups include amines, carboxylic acids,[72] pyridines[73] and fullerenes.[74] Thiol based end groups can be used when a molecule are designed to attach to gold electrodes.[75] It should be noted that the conductance can still vary depending on the microscopic contact geometry and e.g. that the end groups are attached to a bridge, hollow or on-top site on the metal electrodes.[76]

There are several suggestions on how to position single molecules between two electrodes for electronic measurements, however most of the current methods only handles one or a few molecules at each measurement. The number of transistors on a state-of-the-art computer chip is over 100 million per mm^2 [77] and the number of working single electron devices must be able to match this number in order for it to be an interesting future option to conventional semiconductor industry. An idea is to assemble molecules and NPs together and then deposit these on prefabricated electrodes. [43,44]

1.3 Nanoparticle dimers formation and assembly

There are several suggestion on how to assembly NPs together into dimers. One option is to utilize the electrostatic interactions between nanoparticles. Gschneidtner et al. [78] presented a suggestion in 2014 where heterodimers were assembled from negatively charged 2-mercaptoethanesulfonate stabilized gold particles and positively charged cetrimonium bromide stabilized palladium particles. It may be difficult to position single molecules between the particles. It is also possible to combine single particles into dimers by linking them with molecules. DNA e.g., has been used to link NPs since the end of the 1990s. [79,80] The example presented by Bar-Joseph et al. [43] links gold NPs with dithiol particles in order to compares the conductivity of conjugated molecules and molecules with broken conjugation. Another example was introduced by Bjørnholm et al. [81] where gold seeds are linked by poly(ethylene glycol) dithiol and then grown into nanorod dimers. Rods like this could be interesting when depositing them on prefabricated nanostructures in order to achieve control over their direction. Dewi et al. developed a method in 2015 [60] where gold nanoparticle dimers were constructed by first attaching amine terminated terpyridine linkers to a solid support (SiO_2 particles). A second terpyridine linker was then attached to the linkers on the solid support by forming a complex with iron ions. Gold particles were then attached to the newly added terpyridine linker. The iron complex was then removed, separating the particles from the solid support. The gold particles could then, after isolation from the solid support be linked together again into gold particle dimers.

Scientists have already reported that it is possible to link particles together as presented by Jain et al. in 2009 [81] where particle seeds are linked by dithiol-functionalized polyethylene glycol and then grown into dimers. It is also shown that it is possible to electrically measure the molecule linking the particles, for example Bar-Joseph et al. [43,44] where sub 20 nm NPs dimers are linked together with 4,4'-biphenyldithiol molecules, these are subsequently deposited onto one nanogap by electrostatic trapping. This means that only one dimer at the time can be trapped. Other means of deposition was presented by Wolff et al. in 2012 [82] where nanorods were assembled in parallel by microcontact printing. Another example of parallel assembly of NPs is presented in Wolf et al. in 2014. [83] A glass slide is in this example moved over a surface with prefabricated cavities, with a colloidal dispersion between the substrate and the slide, capillary forces are then utilized to depositing the particles in the cavities.

1.4 Research Questions

The general approach of this PhD work is to first isolate single molecules in solution between nanoparticle dimers and second assemble the dimers onto prefabricated electrodes in order to, ideally, be able to construct and measure on multiple single molecule devices in parallel, see fig. 1.3. Finally we want electrically measure on the molecules linking the dimers. We also aim to have a completely parallel process. Nanogaps in that size range can easily be produced by conventional UV lithography and the molecule linked particles are deposited into the nanogaps in parallel.

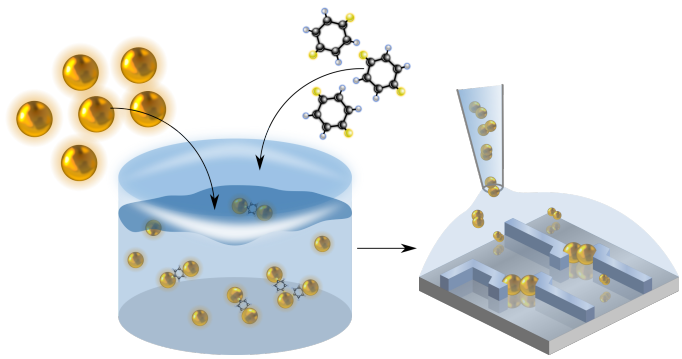

Figure 1.3: *Schematic explaining the method we aim to use in this thesis. Particles and molecules are first assembled in solution and then deposited onto prefabricated nanostructures.*

The main focus point of this thesis is on the deposition of NPs and especially on the assembly and guided deposition of nanoparticle dimers towards molecular electronics. It has already been proven that molecules can conduct current and that depending on their structures can act as for example rectifiers and switches. This thesis will rather focus on the parallel assembly of particles and the optimization of the assembly, without any advanced set-up when doing so. This means that the particles themselves should attach to specific sites without the direct influence of for example electric fields or mechanical stresses. The final goal is to contact molecular linked dimers, or proto-devices, and electrically measure the molecule attacked between the particles. The following questions were therefore asked at the beginning of the research presented in this thesis: Is it possible to contact particles and molecular linked particles in a parallel fashion onto prefabricated nanogaps in such a way that this method can compete with conventional semiconductor based integrated circuits? Subsequently, is it possible to electrically measure current through a molecule linked between two NPs deposited in a way described above, see fig. 1.3? Will the resistance of these measurements correspond to the resistance measured by others using e.g. the break-junction technique?

2 Nanoparticle and surface interactions

This chapter introduces colloidal NPs, how they can be synthesised and applications. It also introduce the established DLVO (Derjaguin, Landau, Verwey and Overbeektheory) theory, explained by Israelachvili in 2011.[84] The DLVO-theory explains the interactions between particles in a colloidal dispersion plus the interactions that the particles affected of when depositing on a surface. The following section will discuss the Monte-Carlo based RSA (random sequential adsorption) process, first introduced in 1958,[85] used to investigate filling factors of objects on a 1D line or 2D area. The ERSA (extended random sequential adsorption) is a combination of the DLVO and RSA, developed by the author of this thesis which is used to simulate the deposition of colloidal NPs onto a surface. The inter-particle distances are then calculated using a spatial descriptive statistic called Ripley's K and L functions[86–88] established in the 70s.

NPs are objects in the size range of around 1-100 nm, they can have round or elongated shapes and exists in a variety of materials. Metal NPs were used in the 15 and 16th century to stain window glass in for example churches.[89,90] However, NPs have a much wider use in areas such as in sunscreen, where metal oxide NPs protect against UV-radiation.[91] Silver particles can act as anti-bacterial agents in textiles and bandages.[92] NPs can also be used in sensing devices[93,94] such as the palladium-gold NPs dimers were used in indirect plasmonic sensing of hydrogen.[95] It has also been shown that NPs can be used in electronic applications such as single electron transistors, where coulomb blockade can be achieved by placing a NPs in the size range of 10 nm between three electrodes.[96,97] There are several methods available regarding NPs production. Nature itself creates airborne NPs in e.g. plant viruses[98] and in connection with natural combustion such as forest fires or volcano eruptions.[99] Metal NP aerosols can be produced using a spark discharge generator.[100] Wet chemistry is also an option when synthesizing metal NPs. The basic procedure is typically based on the reduction of a metal salt using a reducing agent in presence of a stabilizing ligand.[101]

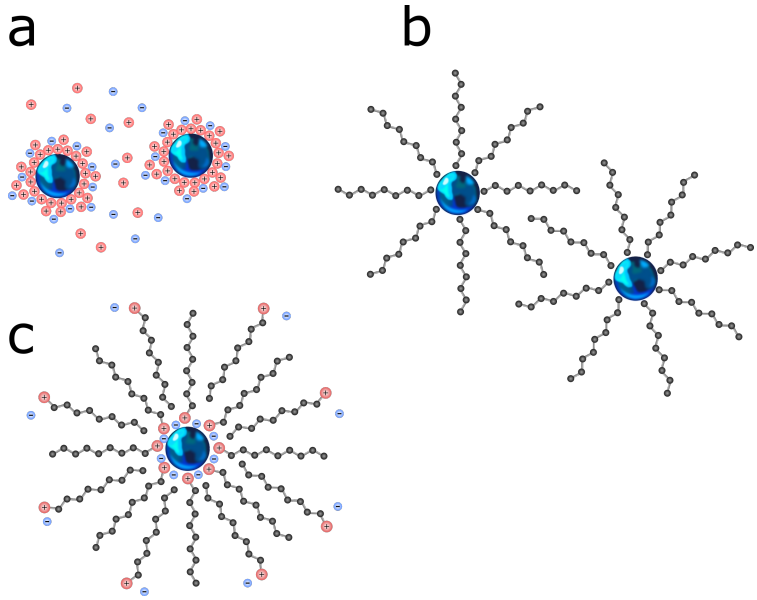

Figure 2.1: *Two schematic examples of NP dispersions stabilized with a) electrostatic (usually found in polar solvents) and b) steric interactions, in this case an alkene chain. c) Corresponds to a surfactant stabilized NP, CTAB is here forming a bilayer around the particles.*

Van der Waals interaction are strong on small objects with a high surface to volume ratio, like NPs. They therefore tend to cluster if they are not stabilized and kept as a dispersion. Different molecules can be used to stabilize them, depending on the dispersion agent. One could e.g. disperse gold NPs in non-polar solvents by coating them with a thiol terminated alkenes.[102] A schematic picture of sterically stabilized particles can be seen in fig. 2.1 b. A thiol is used to attach the ligand to the gold surface.[103] Anchor groups such as carboxylic acids, nitriles and phosphanes, to name a few, can also be used in other metal/metal oxide NPs. Polymers[104] and surfactants[105] are two other examples that could be used to sterically stabilize NPs.[106]

One surfactant commonly used for NPs stabilization is cetyltrimethylammonium bromide (CTAB),[107] which makes it possible to suspend the particles in polar solvents such as water. The CTAB forms a rigid bilayer structure around the particles (see fig. 2.1 c) making them a stable dispersion. It can however be difficult to perform a ligand exchange due to the bilayer around the particles.[108,109] Other options, for aqueous dispersions could be trisodium citrate[110] (see fig. 2.1 a), where the particles are dispersed by electrostatic interaction that appear due to a high concentration of ions close to the particle surface.

Citrate stabilized NPs are easily functionalized with ligands with a stronger bond such as thiolate ligands.[111] These NPs are therefore good candidates for NP dimer formation

where molecules with thiol anchor groups could be attached to form a linkage between two NPs in order to form NP dimers.

NPs are truly a versatile tool in a variety of scientific disciplines. We have discussed different ways of dispersions and applications of them, however it is of great importance to move the particles from the dispersion they were synthesized in, onto some type of substrate for applications such as sensing devices, electronics, biological applications and more. It is therefore interesting to understand how NPs interact with each other and surfaces in order to optimize the deposition of them. This will be discussed in the following section, as well as how one could simulate the deposition of NPs on a surface.

2.1 DLVO-theory, nanoparticle and surfaces interactions

The following part focus on the interactions between particles and surfaces in solution, which is described by the DLVO-theory. This theory was estabilished by Boris Derjaguin, Lev Landau, Evert Verwey and Theodor Overbeek during the first half of the 20th century.[84]

The interactions between two NPs, stabilized with an ion-solution (or a particle and a surface) can be described using DLVO-theory. Two parts are involved; van der Waals attraction W_{vdw} and electrical double layer repulsion W_{edl}, resulting in the combined interactions W_{tot}, where $W_{tot} = W_{vdw} + W_{edl}$.[84,112] A schematic drawing can be seen in fig. 2.2, where an energy barrier arises from the product of the repulsive and the attractive forces. The barrier increases as the distance between the NPs decreases. The particles will attach to each other if they manage to overcome the barrier, provided that they are given enough time, due to the attractive van der Waals forces. The repulsion energy between two NPs in the same dispersion, derived from the electric double layer can be described for small potentials in the following way;

$$W_{edlpp} = 2\pi r\varepsilon_0\varepsilon_r\Psi_p^2 \cdot e^{-\varkappa S} \tag{2.1}$$

Were Ψ_p is the particles surface potential, ε_0 the permittivity in vacuum, εr the relative permittivity of the medium, r the radius of the particles present in the dispersion, $\varkappa$ the inverse of the debye length; λ and S is the distance between the cores of two particles. The repulsion derived from the interactions between a particle and a surface is seen below;

$$W_{edlps} = 4\pi r\varepsilon_0\varepsilon_r\Psi_p\Psi_s \cdot e^{-\varkappa D} \tag{2.2}$$

The van der Waals attraction is described as $-Ar/6D$ between a surface and a particle and $-Ar/12D$ between two particles with the same radius, where A denotes the Hamaker constant.[84] It is possible to approximate the Hamaker constant if the individual Hamaker

constants of the medium, the particles and the surface is known. according to eq. 2.3.

$$A_{123} \approx (\sqrt{A_{11}} - \sqrt{A_{33}}) \cdot (\sqrt{A_{22}} - \sqrt{A_{33}}) \tag{2.3}$$

The systems Hamaker constant A_{123} can be described as a combination of the individual Hamaker constants for the system, where A_{11} is the constant for the particles, A_{22} for the surface and A_{33} is for the medium. The individual constants have been measured using two identical media interacting in a vaccum.[84]

The debye length mentioned in eq. 2.1, 2.2 and 2.10 describes how far the electrostatic interactions reach in a solution, that is how far a particle will feel another particle or a surface in the solution. The debye length can be seen in eq. 2.4, where avogadros constant is denoted by N_A the elementary charge by e, and the ionic strength by I.[84,112]

$$\lambda = \sqrt{\frac{\varepsilon_r \varepsilon_0 k_B T}{N_A e^2 I}} \tag{2.4}$$

The ionic strength is given by; $\frac{1}{2}\sum_i z_i^2 c_i$, where, z_i is the valency and c_i the concentration of the ions in the solution surrounding the NPs.

The surface potential Ψ is defined as the potential difference between the surface of e.g. a particle or a flat surface and the bulk solution. The surface charge of the particle is negative in fig. 2.2 b, hence attracting positive ions, tightly bonded, in the Stern layer. The slipping plane defines the border where ions will move together with the particle as one entity. Ions further away will not move along with the particle.[113]

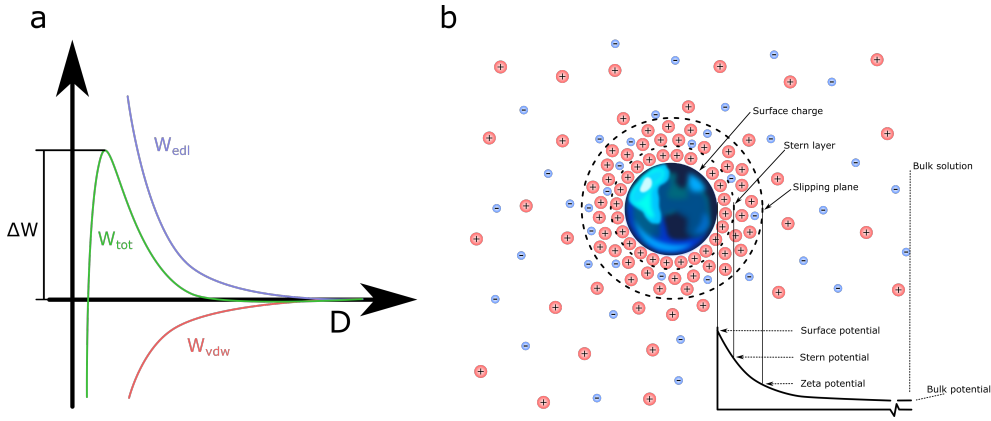

Figure 2.2: *Schematics over (a), the attractive and repulsive forces between two NPs or a NPs and a surface.* W_{edl} *corresponds to the energy from the electric double layer,* W_{vdW} *the energy from the van der Waals interactions and* $W_{tot} = W_{vdW} + W_{edl}$. *The potential barrier height is denoted by* ΔW. *(b), Shows the difference between surface potential, stern potential and Zeta potential.*

The ζ-potential is the potential difference between the bulk solution and the potential at the slipping plane, seen in fig. 2.2, b. The potential cannot be measured directly, however it can be calculated by applying an electric field, the particles will then move along with the ions in the stern layer and the sliding plane according to the field, the movement can then be recalculated into the zeta-potential. ζ-potential measurements in the included work were performed using a Malvern Zetasizer nano system, which uses electrophoretic light scattering to measure and calculate the zeta-potential of a colloidal system.[114] This system can also be used to measure the sizes of colloidal systems such as dispersed NPs using dynamic light scattering.

The DLVO theory explains how colloidal particles such as citrate stabilized NPs interact with each other or with a surface. However it cannot predict the outcome of a deposition, other mathematical expressions is needed in order to do this. One option is random sequential adsorption (RSA) which will be described in the following section.

2.2 Random sequential adsorption

The following section will discuss the RSA (Random sequential adsorption) first presented in 1958 by Alfréd Rényi.[85] This is also called the car parking problem, where he in one dimension investigated how many that will fit along a street, if the cars are parked randomly. The two dimensional RSA, presented by Adamczyk et. al. in 1994[115] and Oberholzer et. al.[116] in 1997, is used to investigate how many ranomly generated particles that can fit on a surface. This section will also discuss the ERSA (extended random

sequential adsorption), where the author of this thesis combined DLVO is with RSA and introducing a new way to simulate the deposition of colloidal NPs on a surface.

The two dimensional RSA is a way to randomly generate particles and putting them on the x,y-coordinate system of a surface. Particles overlapping another particle will be discarded and generate a new particle located at a random x,y-coordinate, it will continue to do so until the number of tries have been reached.

The process can be modified to include particle-particle and particle-surface interaction described by the DLVO theory into the extended-RSA (ERSA) process, presented in paper I.[117] A deposition probability is derived from the height of the barrier (ΔW), seen in fig. 2.2 a, and described by; $P_{ps} = \exp(-\Delta W/k_B T)$. k_B denotes the Boltzmann's constant and T the absolute temperature. The probability for the particle to be rejected in the deposition process increases as the height of the barrier increases. However, particles already deposited on the surface will reject the incoming particle and a second probability is therefore needed. The van der Waal's interactions between two particles are in this case discarded, the probability of finding a particle next to another at the distance $S(P_{pp})$, is described by the Boltzmann distribution $P_{pp} = \exp(-W_{edlpp}/k_B T)$. The probability for a particle to be discarded increases if it tries to deposit near another particle already deposited due to the repulsive forces between two objects with the same surface potential. It will be more difficult for a particle to deposit if many particles already exists on the surface.

The RSA process is Monte-Carlo based and lacks time dependence, since it is not known how long time a particle needs to deposit. However, the number of particles diffusing through a given area in the solution (W), during a given time (t), can be calculated according to eq. 2.5.[118] The nanoparticle concentration is given by C_0, the viscosity of the solvent by η and the duration of the deposition by t. N would then be the number of attempts the RSA process will perform, hence making it time-dependent.

$$N = W \cdot C_0 \sqrt{\frac{t k_B T}{12 \pi \eta r}} \tag{2.5}$$

Fig. 2.3 a, corresponds to a section of a SEM micrograph where citrate stabilized NPs have been deposited on a Si/SiO_2 surface, which have been treated with APTES in order to change the polarity of the net surface potential. The particle density for the whole SEM micrograph is 20.5 NPs/μm^2. A set of ERSA simulations with corresponding surface potentials were then performed, the NP density of the simulated depositions were then compared to the particle density of the depositions performed.

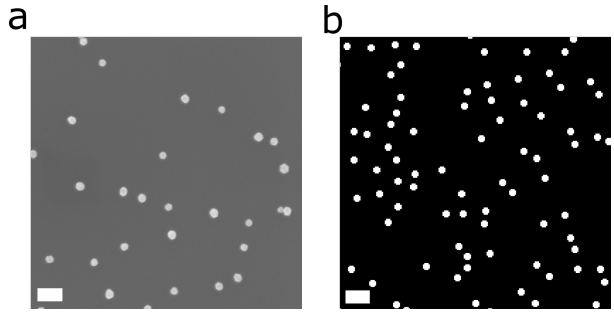

Figure 2.3: *a) SEM micrograph of citrate gold NPs deposited on a (100) Si/SiO_2 wafer. The surface have been treated with 3-aminopropyl)-triethoxysilane (APTES) in order to be able to attract negatively charged particles. b) a pattern that appears after a ERSA simulated deposition of NPs. The white dots represents NPs. The scale bar in a and b corresponds to 200 nm.*

A section of an ERSA simulation example, with a particle density of 18.5 NPs/μm^2 can be seen in fig. 2.3 b, where the white dots represents deposited NPs. The ERSA example had the particle density which fitted best to the particle density of fig. 2.3 a. The particles are evenly distributed throughout the samples in both a and b. Worth noting is that some clustering of two particles can be seen in 2.3 a these are however not present in b. The reason for this lies in the RSA model, where particles that are overlapping is discarded. There seems to be an inter-particle distance present in both images in fig. 2.3, however a more thorough investigation is needed in order to evaluate this further, which will be discussed in the next section.

2.3 Spatial descriptive statistics

The following section introduces the Ripley's K and L-function, which is a classical way of determine if objects in a pattern follows complete spatial randomness, clusters or separates at a certain distance.[86–88] We also explain how the K and L function can be used to extract the inter-particles distances after deposition and from the simulated results.

One way to evaluating the results from ERSA simulations of SEM micrographs of NP covered surfaces would be to compare the number of NPs present per area unit. However, this method will not take the position of the particles into consideration. As an example the number of particles present in fig. 2.4 a/b, are equal, but the particles have clustered in fig. 2.4 a, with a specific distance, both between the particles inside the clusters and between the clusters themselves. The particles in fig. 2.4 b, on the other hand are evenly distributed over the surface. This means that the NP density alone is not a precise way to evaluate the deposition of NPs.

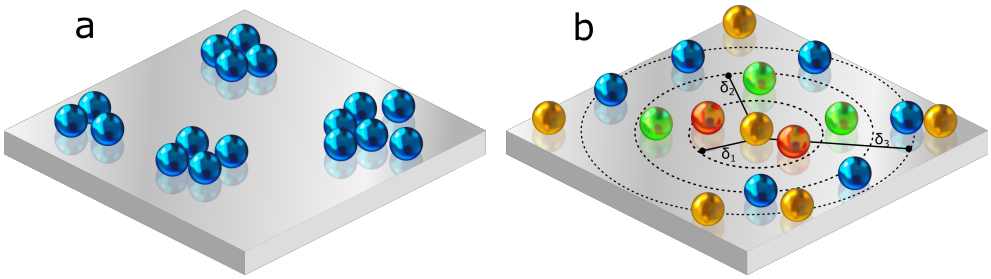

Figure 2.4: *Two schematic examples of how particles can deposit on the surface. The number of particles in both a and b are the same, the NP density are therefore the same. The particles in a, have clustered together with a typical distance between the particles in the clusters and a typical distance between the clusters. The particles in b have a more uniform distribution over the surface, however there seems to be a close range order with an inter-particle distance present. The Ripley's K-function is depicted in b; the sum of particles within a specific distance from one particle is added up for all particles present in a specific area and normalized according to eq. 2.6. Two particles (red) are present within distance* δ_1 *from the golden particle in the middle, five within the distance* δ_2 *(red and green) and ten within distance* δ_3 *(red, green and blue).*

Ripley's K-function,[88] seen in eq. 2.6, is a spatial statistical way to distinguish deviations from complete spatial randomness (CSR). The number of particles within specific distances from a particle particle is summed, this is repeated for each particle throughout the area of interest. An example of this can be seen in fig. 2.4 b, where two particles is closer than the first distance; δ_1, in an array, five within the second distance; δ_2 and ten is closer than the third distance; δ_3.

$$\hat{K} = \hat{\lambda}^{-1} \sum_{i} \sum_{i \neq j} \frac{I(d_{ij} < \delta)}{N} \tag{2.6}$$

The estimated particle density, $\hat{\lambda}$, is calculated by dividing the number of particles, N, with the size of the area of interest. I is unity for all particles fulfilling ($d_{ij} < \lambda$), otherwise zero. The euclidean distance between one point and the rest is denoted by d_{ij} and λ is an array of distances that increases. Ripley's K-function can be reconstructed into Ripley's L-function,[87] see eq. 2.7, in order to emphasize the deviations from complete spatial randomness, corresponding to $\hat{L} = 0$.

$$\hat{L} = \sqrt{\frac{\hat{K}}{\pi}} - \delta \tag{2.7}$$

Positive values indicates that the particles are clustering at that specific distance, negative values in the $\hat{L}$-function indicates that the particles tend to separate at that specific distance.

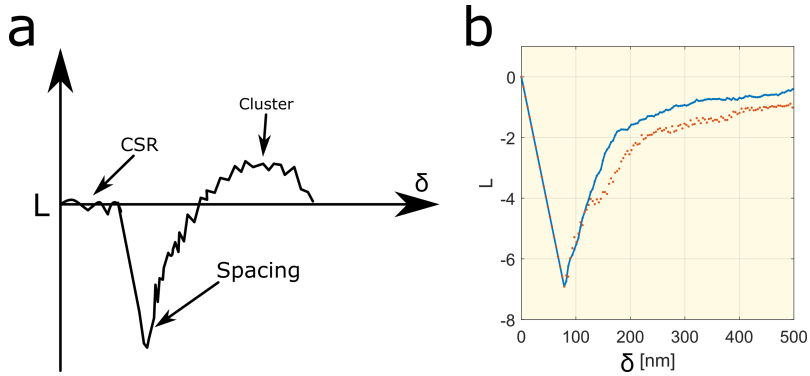

Figure 2.5: *(a) An example of how different L-functions plotted against the distances* δ *and how to interpret the results. Complete spatial randomness is found at neutral values, clustering at positive values and separation at negative values. The Ripley's-L function of the real (blue) and the simulated deposition (red) seen in fig. 2.3.*

An example of how different L-functions can look like can be seen in fig. 2.5 a. The first part represent complete spatial randomness and indicates that there are no order in the pattern. The first negative dips could for instance correspond to the short range order present in fig. 2.4, b. The positive peak would on the other hand correspond to the distance between the clusters in fig. 2.4 a. Subsequently, the L-function goes back to complete spatial randomness indicating that the particles does not affect each other after this distance. It should be noted that the K and L-functions works best for shorter distances.

The L-function for the patterns present in fig. 2.3, where the blue line corresponds to fig. 2.3 a, and the red dots to fig. 2.3 b. The dip around 80 nm shows that there are an inter-particle distance present at that distance, there are however no long range order present in either of the two patterns.

2.3.1 Controlling nanoparticle deposition by surface modifications (Paper I)

The extended random sequential adsorption process and Ripley's K and L-functions were used in paper I,[117] when we tried to evaluate the deposition of NPs suspended in an aqueous solution onto modified surfaces. The results from paper I will be discussed in the following section.

Trisodium citrate stabilized NPs were deposited onto Si/SiO_2 surfaces in the following way; a Si chip was in some of the experiments treated with O_2-plasma and then placed on a scaffold placed in a petri dish with water. A drop of the colloidal dispersion was placed on the chip, followed by closing the petri dish with a lid in order to prevent the drop from drying. The excess of particles were then removed by rinsing the chip in DI water and

dried in using N_2-gas. The experiments showed that it is difficult to attract negatively charged citrate stabilized particles towards a clean Si/SiO_2 surface. The reason for this can be explained by the isoelectric point of SiO_2 (see table 2.2) described in the following section, making it negatively charged at pH neutral, hence repelling citrate stabilized NPs. The Si/SiO_2 surfaces was therefore functionalized with (3-Aminopropyl)triethoxysilane (APTES) and Poly-L-Lysine Hydrobromide (PLL-HBr). N and p doped silicon wafers were used in combination with these two surface modifications in order to see if the doping could affect the deposition in some way. Some samples were prior to the functionalization treated with oxygen plasma. SEM micrographs of the samples after one hour of deposition can be seen in fig. 2.6.

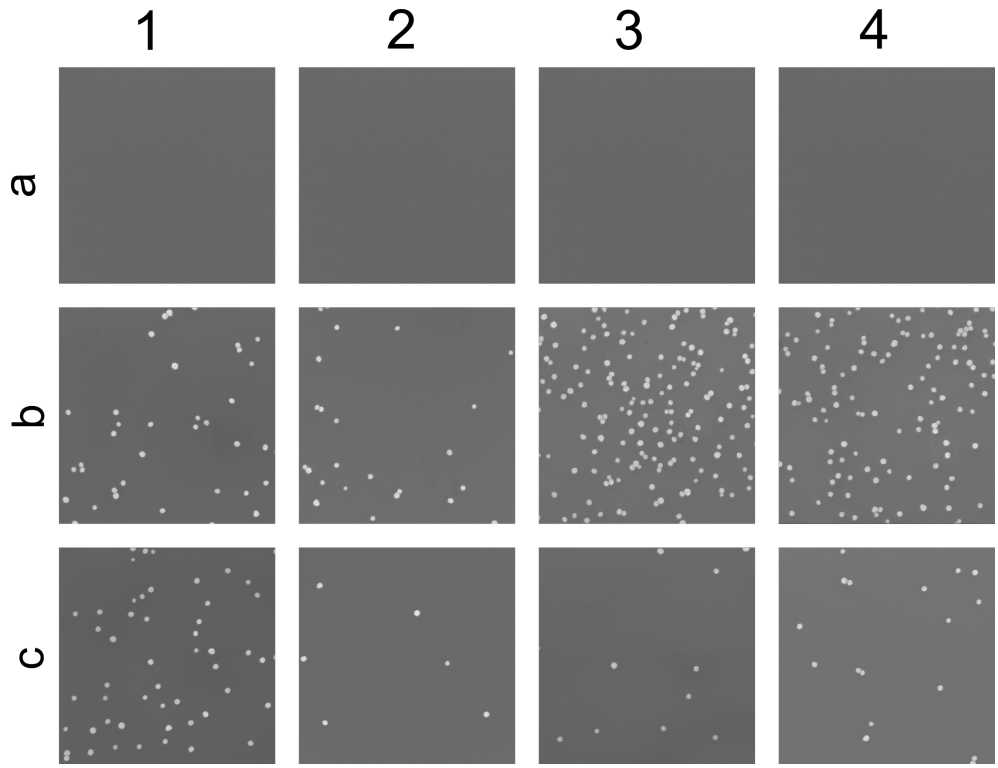

Figure 2.6: *Sections of SEM micrographs after one hour of deposition of trisodium citrate stabilized NPs. Row a represents surfaces without any functionalization. Row b, are surface treated with APTES and row c with PLL-HBr. Column one is n-doped Si, two p-doped Si, three with n-doped Si treated with O_2 plasma and column four with p-doped Si treated with O_2 plasma. (reprinted with permisson from RSC Advances)*

No particles were found on the non-functionalized samples in row a in fig. 2.6. The highest NPs density is found on the sample 3b and 4b. These were the samples treated by first O_2-plasma followed by APTES functionalization, indicating that APTES adhere

Table 2.1: Inter-particle distances from the SEM micrographs in fig. 2.6 and their respective ERSA matching.[117]

	APTES		PLL-HBr	
	Real	ERSA	Real	ERSA
p-doped	100 (± 10.6)	88.3 (± 9.8)	220 (± 60.4)	256 (± 100.2)
n-doped	92 (± 3.5)	85.8 (± 10.8)	98.8 (± 2.8)	85 (± 4.8)
n-doped + O_2 plasma	80.5 (± 2.4)	80.8 (± 1.5)	122.3 (± 19.8)	94 (± 26.7)
p-doped + O_2 plasma	106.8 (± 2.9)	79.3 (± 2.2)	171.3 (± 34.3)	161.8 (± 53.1)

better in those cases compared to 1a and 2a without any O_2-plasma treatment prior to the functionalization of APTES. This might be explained by an increase of silanol groups on the surface after plasma treatment since APTES react with those to form a covalent bond to the surface, or at least a surface with fewer contaminations present, which could hinder the reaction between the silanol groups and APTES. The highest density of the PLL-HBr treated surfaces can be seen in fig. 2.6 1c, followed by 3c, this indicates that the plasma treatment has little effect on the deposition in combination with this treatment. All samples in fig. 2.6 were matched to an ERSA simulation, the particles positions in both the samples in 2.6 and their respective ERSA matching were investigated by Ripley's-L function. The result can be seen in table 2.1.

One can see from the inter-particle distances in table 2.1 that the shortest distance is around 80 nm, this corresponds to fig. 2.6 4b, the n-doped Si treated with O_2-plasma followed by functionalization of APTES, which is also the sample with the highest NP density. This corresponds to the same sample seen in fig. 2.3 a. The ERSA simulation agreed with the measured results and predicted the inter-particle distance in this case. This information was later used when designing patterns used for guided deposition of NPs as it seems difficult to force particles closer to each other than around 80 nm. The ERSA simulation underestimates the inter-particle distance in all cases except the p doped silicon surface treated with PLL-HBr, where it instead overestimates the distance with 30 nm. The reason for this can be due to the fact that the RSA process does not take overlapping particles into consideration, this effect will be more visible for lower NP densities such as in fig. 2.6 2c, which also has the lowest particle density of all samples, except the non-functionalized ones in fig. 2.6.

2.4 Surface charges (Paper I and Paper II)

We have at this point discussed the interactions between particles within a colloidal dispersion and interaction between particles and surfaces, and how the ζ-potential can be used to evaluate the charge and stability of a dispersion. This section will discuss how one can measure the surface potential of a larger surface, and how the conditions of the dispersion will affect the surface charge.

The point of zero charge (PZC), which is sometimes referred to the isoelectric point (IEP), is a material property that is used to determine at what pH a surface has a net neutral charge. The surface will receive a negatively net charge at pH above the IEP due to build up of hydroxide ions (OH^-) and a positive net charge at pH below the IEP due to the build up of hydronium ions (H_3O^+). The IEP for different oxides can be seen in table 2.2

Table 2.2: IEP of different metals.[119–121]

metal/metaloxide	Al_2O_3	NiO	CuO	V_2O_5	SiO_2	Au
IEP	8.7	12	9.5	1.4	3.9	5.2
Charge at pH 7	+	+	+	-	-	-

A substrate made of Si covered with an oxide layer of SiO_2, would according to the values in table 2.2 be attractive for positively charged NP dispersions (stabilized with e.g. CTAB) at pH 7 and repulsive for NP dispersions (stabilized with e.g. citrate). This can be seen in fig. 2.7 where positive charged NP attached to the surface in a and where the citrate stabilized NP are absent in b.

A metal surface such as Al forms a protective layer of Al_2O_3 at ambient conditions,[122] Si is also known to form one type of stable oxide SiO_2,[123] and Au does not form any oxides at ambient conditions due to its noble nature. However, other thin film metals can form a variety of oxides at ambient conditions.[124–126] It is therefore not trivial to guess the surface charges of metal/metal oxides from just the IEP values, other methods must therefore be utilized in order to evaluate the surface charge of different metals and hence usefulness as substrates when depositing NPs.

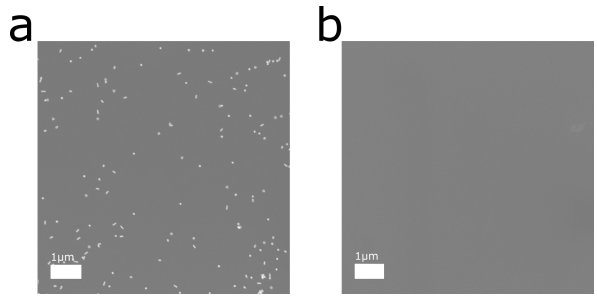

Figure 2.7: *SEM micrographs of two Si/SiO_2 surfaces. a is deposited with CTAB stabilised NPs, b is deposited with citrate stabilized NPs.*

The surface work functions,[127] φ_{sample} (paper I) of the samples seen in fig. 2.6 were measured and calculated (using eq.2.8) prior to the deposition of NPs by a kelvin probe force microscope (KPFM).

$$\varphi_{\text{sample}} = \varphi_{\text{ref}} - e\left(\Delta_{\text{cpd,tip–ref}} - \Delta_{\text{cpd,tip–sample}}\right) \tag{2.8}$$

The known work function of gold is denoted by φ_{ref}, e is the elementary charged, $\Delta_{\text{cpd,tip–ref}}$ is the contact potential difference measured on a gold reference sample and $\Delta_{\text{cpd,tip–sample}}$ is the measured contact potential difference of the samples in fig. 2.6. The measured work functions vs. the NPs densities (based on the SEM micrographs in fig. 2.3) of the corresponding samples can be seen in fig. 2.8 plus the surface potential of the ERSA simulations vs. their surface potential.

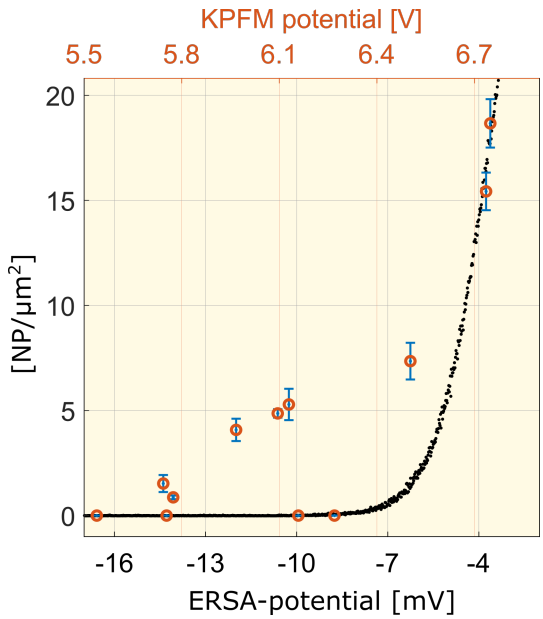

Figure 2.8: *The workfunctions from eq. 2.8 vs. the NPs densities, seen as red, can be red from the top x-axis. The ERSA simulations vs. the surface potentials, seen as black, can be red via the bottom x-axis (reprinted with permission from RSC Advances).*

One can see that the simulated ERSA densities are increasing exponentially as the surface potential decreases, however the KPFM potentials are not following the ERSA data-points exactly, one explanation is due to the fact that the KPFM measurements were performed in air, ions such as sodium, citrate, hydronium and hydroxide will affect the measurements. One should also keep in mind that the KPFM gives the surface work-function which is the amount of energy it takes for an electron to be exited into vacuum. The surface potential on the other hand is the potential difference between a surface and the bulk solution.

There are examples where scientists have performed KPFM-measurements in water.[128] Another approach for evaluating the surface charge have been employed in Paper II. It should be noted that the AFM measurements below and the calculations performed based on eq. 2.9-2.12 have been performed by Mikkel Herzberg at the University of Copenhagen.[129] The force curve from AFM measurements are here fitted according

to DLVO theory. An AFM gold tip were coated with a self assembled monolayer of undecanethiol. This to protect it from accumulating charges and let it approaches a surface of interest in a liquid environment similar to the one in which the colloidal NPs are suspended in.[129] The following eq. 2.9-2.11 explains the DLVO theory which the experimental force curve are fitted to.

$$F = \int_{\infty}^{0} f_e \cdot 2\pi vdW + \int_{\infty}^{0} f_{vdW} \cdot 2\pi rdr \tag{2.9}$$

The geometry of the tip, dr, is described by Drelich et. al. in 2007.[130] The electrostatic force is described by eq. 2.10.

$$f_e = \frac{2}{\varepsilon_0 \varepsilon_r} \cdot (\sigma_t \sigma_s e^{-D/\lambda} + (\sigma_t^2 + \sigma_s^2) \cdot e^{-2D/\lambda}) \tag{2.10}$$

Here, λ denotes the debye length, D, the distance between the substrate and the surface, σ_t the charge of the tip and σ_s the surface charge of the substrate. The vacuum permittivity is denoted by ε_0 and ε_r the relative permittivity of the medium in which the colloidal particles are dispersed in. The van der Waals force is described by the equation below.

$$f_{vdW} = -\frac{A}{6\pi D^3} \tag{2.11}$$

One could in this manner extract the surface charge density at the surface, which into turn can be converted to a surface potential by the Grahame equation, (eq. 2.12).

$$\sigma_s = \sqrt{8\rho_0 \varepsilon_r \varepsilon_0 \varkappa_B T} \cdot \sinh \frac{ze\Phi - 0}{2k_B T} \tag{2.12}$$

The valency of the ions used to stabilize the NP dispersion is denoted by z and ρ_0 is the ion concentration. The surface potential of the substrate in question is Φ_0.

The drawback with this methods is that the exact conditions of the medium needs to be known in order to extract good fits of the force curves into surface potential. Another drawback with this method is that one will not know the sign of the calculated surface potential. The sign of the potentials, of the potentials vs. the NP density in fig. 2.11, is assumed positive for copper, nickel and aluminium and negative for gold, Si/SiO_2 and vanadium.

The structures that were used in the AFM surface charge measurements (paper II) plus corresponding NP deposition can be seen in fig. 2.9. The hexagonal structures are around 1.2 mm across. Each section of the hexagonal shaped structures consists of vanadium (V), nickel (Ni), copper (Cu), aluminium (Al) and gold (Au). The final hexagonal section is left empty in order to expose the SiO_2 underneath. An XEDS (X-ray energy dispersive spectroscopy) map, confirmed the elements in fig. 2.9. The oxide compositions is still unknown, this can however be solved by performing an XPS (X-ray photoelectron spectroscopy) measurement of the structures.

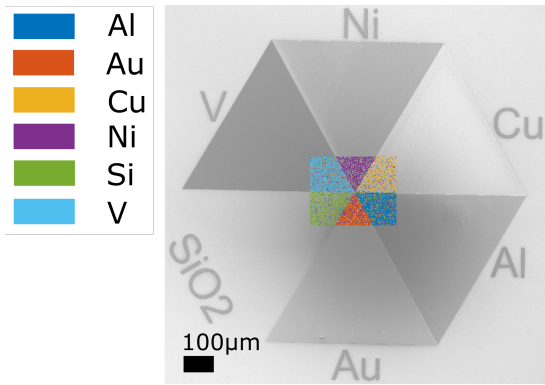

Figure 2.9: *SEM micrograph over one of the hexagon structures used for NP deposition and for surface potential measurements. An XEDS map is inserted in the middle of the structure confirming the elements used in the experiments. Each section of the hexagon is label with the corresponding material (reprinted with permission from EPL).*

The following procedure were used when depositing particles on the structures in fig. 2.9. Citrate stabilized gold NP were deposited for one hour on an array of structures seen in fig. 2.9, SEM micrographs of the result is seen in fig. 2.10. The same deposition procedure were used here as in the paper I, a drop of the colloidal dispersion was placed on a chip of Si/SiO_2. This chip was placed on a scaffold inside a petri dish filled with DI water in order to preventing the dispersion to evaporate. The chip was then rinsed in water and dried in N_2 gas before SEM measurements.

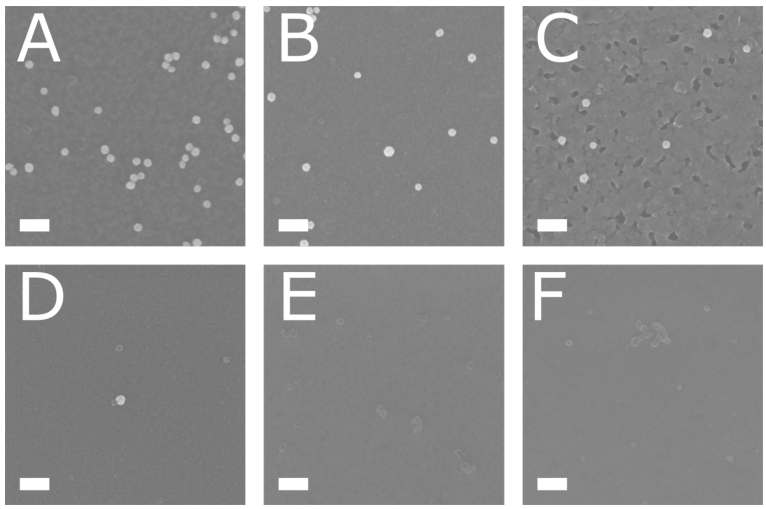

Figure 2.10: *parts of SEM micrograph over the sections of the hexagonal structure can be seen in fig. 2.9. A represents Aluminium (Al), B: nickel (Ni), C: copper (Cu), D, vanadium(V), E: silicon (Si/SiO_2) and F: gold (Au). The scalebar is 200 nm (reprinted with permission from EPL).*

One can directly from both the SEM micrographs in fig. 2.10 and the plot in fig. 2.11 see that the highest density is found on the aluminium section (A in fig. 2.10 and 2.10) followed by nickel (B) and copper (C). No particle can be seen in the vanadium (D), Si/SiO_2 (E) or gold (F) sections. It is expected to see a small or no amount of NPs for Au, V and Si/SiO_2 due to the fact that their (or oxides that forms from these materials) IEP or PZC (see 2.2) is well below the pH of the solution surrounding the NPs. It should be noted that other oxides than V_2O_5 might of course be present on vanadium. However the measured and calculated surface potentials of V, Si/SiO_2 and Au is below the ζ-potential of the NP solution (-35.96 mV) which explains why the particles are repelled from the surfaces in these cases. It is also expected that we find NPs on Al, Cu and Ni, due to the fact that their IEP is above the pH of the NP dispersion. It is a bit surprising that the highest density can be found on the Al sample, the IEP of Al_2O_3 is lower compared to both Ni and Cu. However the Al sample have the highest surface potential in the plot seen in fig. 2.11, the difference between the surface potential of Ni is however not that big, only 3.5 mV and 17 mV between Al and Cu. Al quickly forms a protective oxide of

Al_2O_3 in ambient air. Ni and Cu can on the other hand form other oxides than the ones presented in table 2.2.

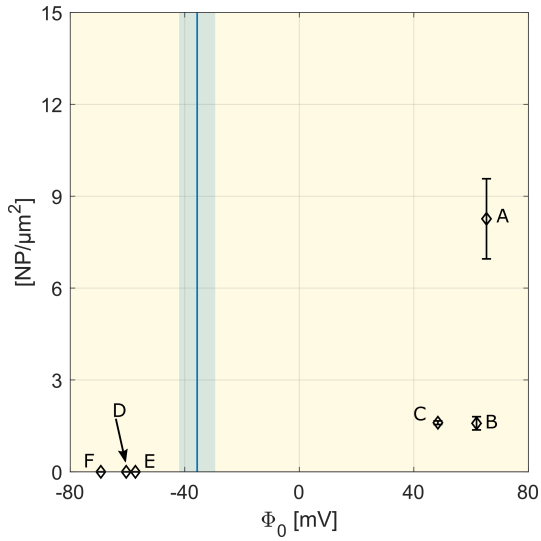

Figure 2.11: *A plot showing the NPs density vs. the surface potential measured by the AFM force curve fit for the surfaces in fig. 2.10. The annotation are the same in this plot as in fig. 2.10. The blue line represents the mean zeta-potential (–35.96 mV) measurement of the NP dispersion and the blue area the zeta-potential standard deviation (±10.9 mV) (reprinted with permission from EPL).*

3 Directed Self-Assembly of nanoparticles.

Previous chapters have discussed the deposition of particles on surfaces, however in the context of this thesis it is necessary to guide the particles and molecular linked dimers towards specific sites if they are going to be integrated in an electric grid. This chapter will therefore treat the guided deposition of particles and molecular linked particle dimers. We will first discuss different techniques used by others in order to guide or direct particles during a deposition process. This will be followed by the results in paper III and IV, which focuses on the optimization of deposition of NPs on nanostructures, and additionally some unpublished results, regarding this topic. This will be followed by the development of nanogaps, from paper III and IV and finally the evolution of nano electrodes. The assembly of molecular linked dimers and some electrical measurements through a molecular linked dimer, proto-device, from paper III is also included.

Self-assembly is a process where objects organizes themselves from a disordered state into an ordered state without direct human intervention.[131] Several examples of this exists in nature and chemistry such as the formation of cell membranes[132] or DNA complexes.[133] Other examples includes the arrangement of self-assembled monolayers[134] and even crystal growth can be categorized as self-assembly.[135] Self-assembly is sometimes referred to as a bottom-up production method, where small objects are assembled into a larger structure or system. The opposite would then be the top-down method, examples here includes the traditional lithographic and etching methods present in conventional clean room facilities.

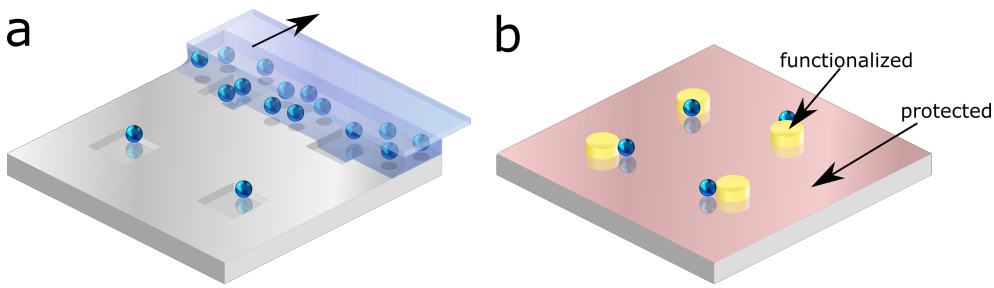

Figure 3.1: *Two ways of direct the deposition of NPs. A glass slide is, in a) moved over a substrate with prefabricated nano cavities. A colloidal dispersion is sandwiched between the glass slide and the substrate creating a meniscus flow when the glass slide is moved over the surface, capturing NPs. The glass slide moves towards the arrowhead. b) The substrate is protected with a lipid bi-layer and the gold is functionalized with 2-mercaptoethanesulfonate making the gold negatively charged hence attractive for the positively charged CTAB NPs.*

We have at this point only covered the deposition of NPs on different surfaces and ways to describe the deposition process. There are however a number of methods to guide or direct the NPs towards specific sites on a substrate. One way is to create a meniscus flow over a substrate with pre-fabricated cavities,[83,136] the setup can be seen in fig.

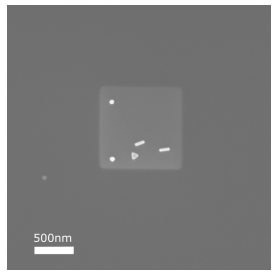

Figure 3.2: *SEM micrograph of CTAB stabilized Au-NPs deposited into an opening of a PMMA coated Si/SiO_2 wafer.*

3.1 a. Other methods includes electrostatic trapping, where an electric field is applied between pre-defined electrodes to attract colloidal particles.[44] It is chemically also possible to activate specific parts and protect others in order to direct the deposition of NPs, see fig. 3.1 b. One example of this method was presented by Fernandez et. al.[137] in 2014, where gold nanodiscs on a Si/SiO_2 surface were functionalized with a layer of sodium 2-mercaptoethanesulfonate. Subsequently, the substrate was then protected by a lipid bi-layer. CTAB stabilized NPs were then directed to the functionalized metal discs. The Bilayer shielded the attractive forces between the positively charged NPs and the negatively charged surface. 2-mercaptoethanesulfonate was bonded to the gold objects on the surface making them negatively charged and attractive for the positively charged, CTAB stabilized NPs. Other methods of directed assembly of particles is the one presented by Sayin et. al. in 2017.[138] Negatively charged gold NPs were in this example directed into positively charged poly(allylamine hydrochloride) cavities, surrounded with negatively charged poly(sodium-4-styrenesulfonate), all prepared using hole colloidal lithography.

Experiments have shown that it is also possible to direct the CTAB coated NPs by using a coating of PMMA(poly(methyl methacrylate)) with developed cavities exposing the Si/SiO_2 substrate, see fig. 3.2. PMMA acts probably as a protective layer similar to the lipid bilayer in the example presented above.

However as explained previously, CTAB can be challenging to work with due to the difficulties with molecular exchange in future experiments. Trisodium citrate stabilized NPs was instead used in the experiments that followed. Another advantage of citrate stabilized NPs is the fact that they are negatively charged (as seen in fig. 2.11), which means that a substrate such as Si/SiO_2 will repulse citrate stabilized NPs, (as seen in fig. 2.6), a protective lipid bilayer is therefore not needed in this case. Molecules such as APTES and PLL-HBr can be degraded in the process of fabricating nano sized electrodes for further electrical measurements, however results seen in fig. 2.10 shows that surfaces such as aluminium and nickel attracts citrate stabilized NPs. It would therefore be interesting to investigate the deposition of citrate stabilized NPs on nanosized objects made of the metals which attracted NPs in fig. 2.10.

3.1 Fabrication scheme, deposition set-up and

The following section describe the procedure used to fabricated the nanosized features as well as the set-up used to deposit NPs in paper I-IV. This will be followed by discussing the results regarding the deposition of NPs and NP dimers.

3.1.1 Fabrication of nanosized features

The following procedure was used when fabricating the nanosized features used in paper III and IV. A double layer resist system consisting of a 100 nm thick lift-off resist (MCC NANO Copolymer EL6, Microlithography Chemicals Corp.) followed by a 50 nm thick electron resist (ARP 6200.13:Anisol 1:2, Allresist GmBH) was used when fabricating the nanosized features and electrodes in this thesis. The resist system was exposed with a focused electron beam (using an EBL-JEOL JBX 9300FS operating at 100kV), according to a predefined pattern, fig. 3.3 a. The exposure makes it possible to dissolve or develop the electron resist with *o*-Xylene. A mixture of DI-water:2-propanol (7:93), was used to dissolve the lift-off resist creating an undercut (fig. 3.3 b). Subsequently, metal layers, with a defined thickness, were evaporated onto the sample using a Lesker PVD 225 system, fig. 3.3 c. A lift-off in acetone dissolved the lift-off resist and removed the evaporated metal, fig. 3.3 c, leaving the nanosized objects on the substrate, fig. 3.3 d. A double layer resist system (0.3 µm LOR3A and 1.5µm S1813) was also used when constructing the larger structures such as the hexagons seen in fig. 2.9 and for the parts used to contact the electrodes in fig. 3.13. A laser writer (l=405 nm, Heidelberg Instruments DWL 2000) was used during the exposure, and MF319 was used as developing agent.

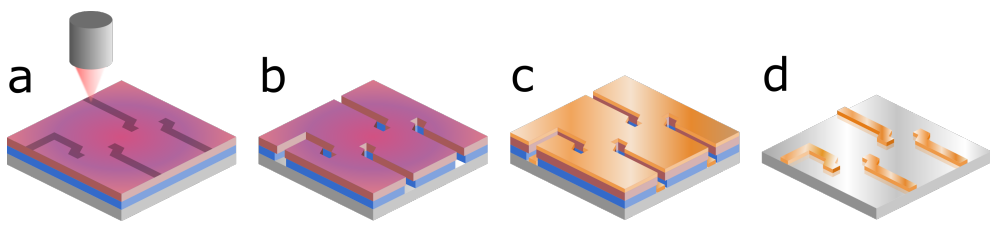

Figure 3.3: *A schematic overview of the nanoelectrode production. a) The double layer resist (lift-off resist in blue, electron resist as purple) is exposed to a focused electron beam. b) Development agents, in two steps, are used to develop the pattern. c) Layers of metals are evaporated at a specific thickness, several metals can be evaporated at this step. d) A lift-off agent dissolved the bottom lift-off resist and removes the excess metal, leaving the metal objects.*

3.1.2 Deposition set-up

The following section explains the set-up used when depositing NPs in paper I-IV. The chip was placed on a 3D-printed scaffold in a petri dish filled with the same mixture of H_2O:2-propanol as present in the drop, in order to saturate the local environment, hence suppressing the evaporation of the drop containing the colloidal dispersion, see fig. 3.4. The access of particles were rinsed away in 2-propanol and water followed by N_2-drying.

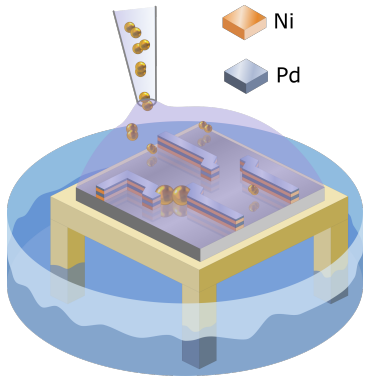

Figure 3.4: *A schematic overview of the setup used when depositing nanoparticles and nanoparticle dimer. The features in this examples is nanoelectrodes consisting of layers of Ni and Pd. (reprinted with permission from small)*

3.1.3 Optimizing the deposition of nanoparticles and nanoparticle dimers (Paper III).

The following section concerns the results in paper III. It was investigated how the deposition of NPs varied on nanosized objects (the majority in nickel) and how parameters such as deposition time and the addition of 2-propanol would affect the deposition.

Sections of two SEM micrographs can be seen in fig. 3.5, where citrate stabilized NPs were deposited on a Si/SiO_2 substrate for 2 h. These first experiments shows that it is possible to direct NPs towards metal objects with an IEP above the pH level of the colloidal dispersion, and that they do not attach to the substrate.

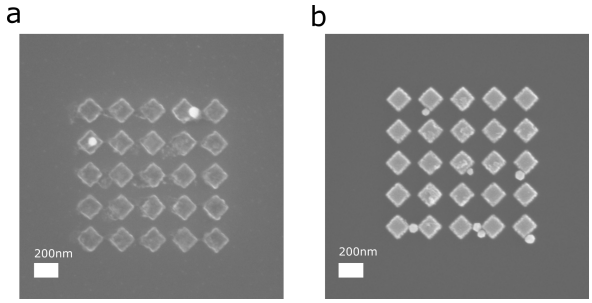

Figure 3.5: *SEM micrographs of prefabricated nanosized structures made from, a) aluminium and b) nickel, on a Si/SiO_2 surface, with citrate stabilized NPs, deposited for 2 h.*

Aluminium should according to the results in fig. 2.10 and 2.11 be better at attracting NPs compared to nickel, however this is not the case in fig. 3.5. Nickel was therefore used in the experiments from this point forward. The number of particles is however still too low. Arrays with a variety of geometrical objects were therefore tested in order to see if the particles favoured any features in the deposition, (this results can be seen in the supplementary information in paper III). An array of five pointed stars of Ni (70 nm thick) with citrate stabilized NPs (deposited on for 2 h) is seen in fig. 3.6.

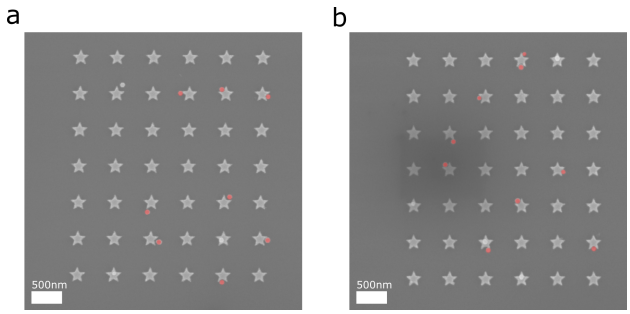

Figure 3.6: *Section of SEM micrographs with arrays of five pointed star shaped objects in nickel. Citrate stabilized NPs have been deposited for 2 h in a) and 24 h in b). The particles considered as correctly deposited is highlighted in red.*

A comparison between different objects were investigated in paper III. The percentage of successful depositions (PSD) of particles, was defined as the number of successfully deposited particles divided by the total number of objects in that specific array. There are 42 stars present in the array in 3.6 a, and eight particles considered as successfully deposited, highlighted as red, this gives a PSD of 19 %. Clustered particles and particles sitting on-top of a structure are not considered as successfully deposited. An increase of the deposition time to 24 h can be seen in fig. 3.6 b. The PSD of NPs were increased to 21 %. Higher PSD of NPs is necessary in order to be useful in further experiments

with dimer deposition. The number of NPs are much lower when depositing them on nanosized objects compared to large surfaces as seen in fig. 2.6 and 2.10. One explanation to this could be due to the powerful repulsion forces between the Si/SiO_2 substrate and the NPs. The particles were rejected by the substrate before they could feel the attracting forces of the nanosized nickel objects. One way of decreasing the interaction between the substrate and the particles was to change the conditions of the solution surrounding the NPs. The debye length (eq. 2.4), could be decreased by changing the dielectric constant or the relative permittivity (ε_r) of the medium of the colloidal dispersion. The addition of 2-propanol to water will according to Park et. al.[139] decrease the dielectric constant of the mixture, hence decreasing the debye length. 2-propanol was therefore added to the NP dispersions prior to the deposition in order to improve the deposition process.

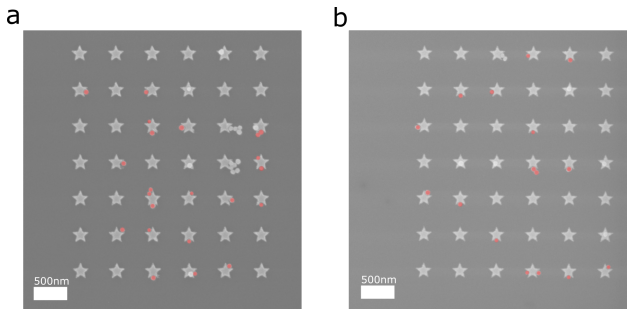

Figure 3.7: *Section of SEM micrographs with arrays of five pointed star shaped objects in nickel. Citrate stabilized NPs have been deposited for 1 h in a) and 4 h in b). A mixture of 4:1 2-propanol:dispersion was used in a and a mixture of 5:1 in b). The particles considered as correctly deposited is highlighted in red.*

The PSD of particles in fig. 3.7 a and b, with 2-propanol present, show a higher PSD of NPs compared to the PSD of particles in fig. 3.6 The difference in PSD of NPs between a and b in fig. 3.7 is not that significant indicating that higher times might be needed in order to achieve higher PSD of NPs. A variety of star arrays with four to ten points were tested at the same time as the five pointed stars presented in fig. 3.6 and 3.7. The PSD of NPs for all of these can be seen in fig. 3.8.

One can clearly see from the plot in fig. 3.8 that the PSD of NPs increases significantly for all star shapes when increasing the deposition time from 2 to 24 h. The PSD of NPs increases further when 2-propanol is added to the colloidal solution. Worth noting is that the particles seems to favour stars with five and six points. The angles between the arms in those cases must therefore match the size of a NP. The difference between 1 h deposition time with 4:1 2-propanol:dispersion and 4 h deposition time and a mixture of 5:1 is not that large indicating that longer deposition times or more 2-propanol is needed in order to see a significant change.

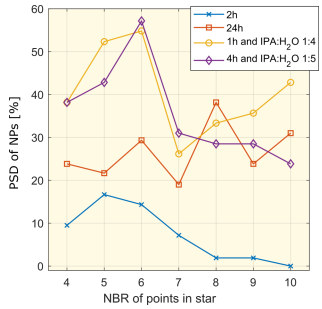

Figure 3.8: *The PSD of NPs vs. the number of point in a star.*

The nanosized objects seen so far has only been used to investigate if it is possible to guide NPs towards specific parts of a surface. The main goal of the thesis is to capture NPs combined with molecules on electrodes and then measure current through them. The deposition on nanogaps, which in principle could be extended into electrodes, was therefore pursued. The angle between two points of the five pointed stars in fig. 3.6 and 3.7 was use as inspiration when designing the nanogaps.

3.1.4 The evolution of nanogaps (Paper III and IV)

So far, we have discussed the directed assembly of nanoparticles onto nanosized objects at surfaces. None of these can be used to electrically contact a particle or a molecular linked dimer. Two electrodes is needed, however it is important that the design of these is optimised in order to increase the number of molecular linked dimers that can be contacted in the end, since the measurement through a molecule linked between two particles is the aim of this thesis. Parameters such as distance between the electrodes and shape was investigated in paper III and IV, but also the duration of the deposition as well as the amount of 2-propanol mixed in the dispersion.

It was investigate if the distance between two objects could affect the deposition, this was done firstly to see if there were a distance that could maximize the numbers of NPs present near a nanosized object, and secondly to understand at what distance two electrodes could be positioned without interfering with each others.

The arrays of two types of nanogaps seen in fig. 3.9 and the analysis of them is included in paper IV. Only sections of the micrographs are shown. Two parallel bars, with a distance of 50 nm, in fig. 3.9 a and b, and two opposing forks, with a distance of 60 nm, in fig. 3.9 c and d. Each array consisted of 70 gaps. The number of particles increases significantly as the amount of 2-propanol is increased (b and d in fig. 3.9) even if the duration of the deposition is decreased from 87 h to 17 h. This is consistent with the results seen in fig. 3.8. It should be noted that the particles sitting outside the nanogap, plus on-top of any structure in fig. 3.9 are not considered as successfully deposited. Larger clusters, such as the one seen in the top of fig. 3.9 d, is not taken into account when calculating the PSD of NPs.

The arrays in fig. 3.9 are parts of a series of arrays, each consisting of 70 elements, with an increasing distance between the objects per array. The PSD of capturing single, double, triple or more particles vs. the nanogap distance can be seen in fig. 3.10.

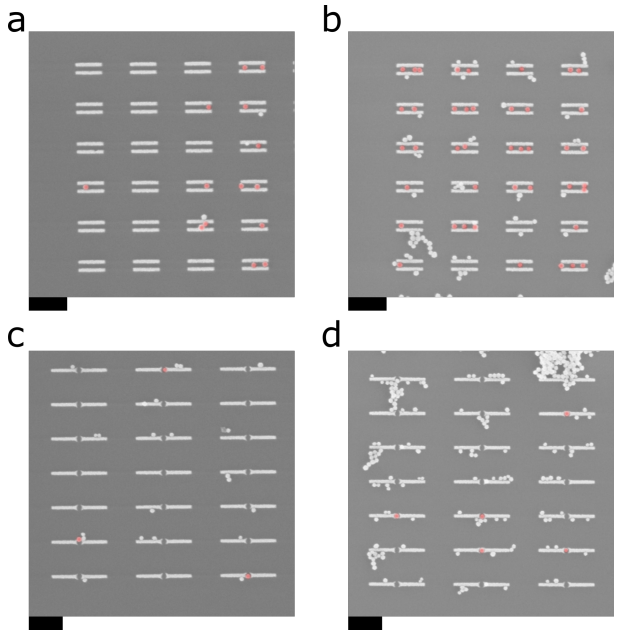

Figure 3.9: *Sections of SEM micrographs, showing arrays of two types of nanogaps, two parallel bars a, b) and two opposing forks c, d). A deposition time of 87 h and a mixture of 1:1, NP dispersion:2-propanol was used for a) and c). A deposition time of 17 h and a mixture of 1:2, NP dispersion:2-propanol was used for b) and d). The scale bars corresponds to 500 nm. Particles considered as successfully deposited is highlighted as red.*

The highest PSD for single NPs (43 %) is seen for the parallel bar structures with a distance of 50 nm and a mixture of 1:1 NPs dispersion:2-propanol, fig. 3.10 a. The PSD for double particles are around 10 % or lower for all gap distances and zero for triple or more. The PSD for single particles (fig. 3.10 a) is then decreasing as the distance increases, indicating that the attractive forces between the dispersed particles and the prefabricated structures increases if they are close enough. Two objects sitting close to each other also gives an increase in interaction area preventing the particle from being re-dispersed into the colloidal again. The PSD of double and triple NPs is significantly increased, to the same levels as the PSD of single particles, when the amount of 2-propanol is increased (see fig. 3.10). This means that the selectivity of only capture single particles is decreased for structures such as the parallel bars when the amount of 2-propanol gets too high. The same trend, where the PSD of single particles are highest for smaller nanogaps, can be seen for the opposing forks, however it is not as clear as in the case of the parallel bars, see fig. 3.10 c. The selectivity for the opposing forks are still present when adding more

2-propanol, fig. 3.10 d, where the PSD of double and triple NPs are kept suppressed. The PSD of double NPs are somewhat increased but is still lower from the PSD of single particles.

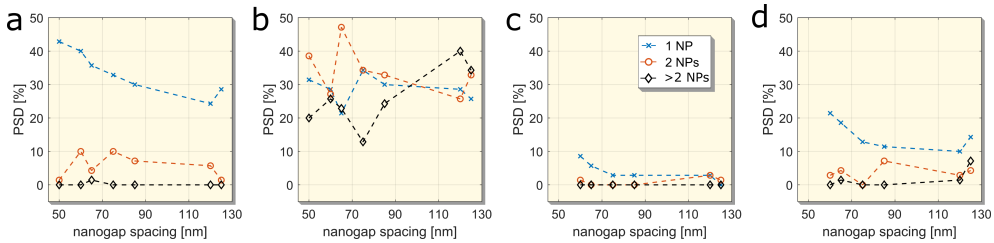

Figure 3.10: *PSD NPs vs. the nanogap distance. The SEM micrograph in fig. 3.9. A deposition time of 87 h and a mixture of 1:1, NP dispersion:2-propanol was used for a) and c). A deposition time of 17 h and a mixture of 1:2, NP dispersion:2-propanol was used for b) and d). The blue data points corresponds to the PSD of single NPs, the red to double NPs and black data points to three or more NPs.*

It is of course important to remember that the final goal is to be able to conduct current through the particles attached to the prefabricated nanogaps seen in fig. 3.9, which is possible by implementing the designs seen previously and then use them as template when fabricating real electrodes. The parallel bar gap seems efficient if it is of interest to capture single particles. However it can easily be short circuit in the system if two or more particles are captured in the same gap. The opposing forks on the other hand, have great selectivity for single particles, both for lower and higher amounts of 2-propanol. A combination of the parallel bars and the opposing forks gave rise to a new generation of nanogaps seen in fig. 3.11.

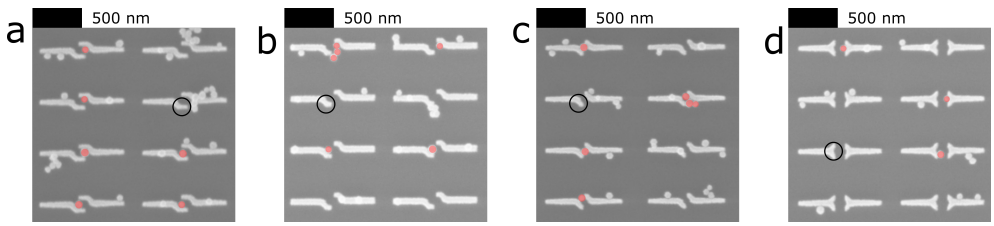

Figure 3.11: *Sections of four SEM micrographs with NPs deposited on them. The same NPs dispersion:2-propanol mixture of 2:1 was used for all four arrays. The deposition time was set to 72 h. Each electrode set is equipped with arms, marked with the rings, they are longest in a), a bit shorter in b) and shortest in c). d) has two contact arms.*

The nanogap arrays in fig. 3.11 consist of 70 elements, a mixture of 2:1 dispersion:2-propanol and a deposition time of 72 h was used for all examples in fig. 3.11. The gaps in this version was equipped with arms (one per electrode in fig. 3.11 a-c and two per electrode in 3.11 d) in order to increase the side area of the electrodes, hence increasing

Table 3.1: PSD of NPs in [%] calculated from the arrays presented in fig. 3.11.

	1 NP	2 NPs	$\geq$ 3 NPs
a	31	1.4	5.7
b	26	1.4	4.3
c	20	4.3	4.3
d	16	3	2.9

the attraction between the objects and the NPs. The PSD of NPs for the arrays in fig. 3.11 can be seen in table 3.1.

The nanogaps in fig. 3.11 a, has a PSD of single particles at 31 % , which is the highest when comparing the nanogaps in fig. 3.11. This is lower compared to the parallel bars in fig. 3.9. The risk of short circuit is still high when depositing dimers, due to the long contact arms which is overlapping each other in one dimension. The contact arms are shorter in fig. 3.11 b in order to prevent the short circuit of dimers. Array d, have two short contact arms per electrodes, this design is not efficient enough and is therefore discarded when continuing the development of arms. Fig. 3.11 c, were designed to capture and contact single particles. Design b and c were therefore used as a inspiration when drawing the electrodes.

3.1.5 The evolution of electrodes (paper III)

With prototype electrode structures at hand (fig. 3.11), a next progression was to develop electrodes with an electronic connection between the nanoscale and the macroscale world. Nickel was again chosen when constructing the electrode nanogaps. The first generation of electrodes can be seen in fig. 3.12 a. The sample consists of 60 nanogaps and four closed reference samples, used to control that it is possible to conduct current through the device. Only four nanogaps fits in one SEM micrograph due to restrictions in the measuring tool used. The PSD of NPs of the array, which fig. 3.12 is part of, is 42 %. However, electrical measurements showed that it was not possible to conduct current through the references wire seen in fig. 3.12 b. The calculated resistance of the reference wire was 50 Ω and the measured resistance for the reference was 8 orders of magnitude higher. The extreme resistance might be due to the production method of electrodes. The electrodes are produced in two steps, the smaller electrode features, such as those seen in fig. 3.12 are deposited first, followed by larger parts of the electrodes made of titanium and gold, which is used to contact the electrodes when conducting current thorough it. Nickel will produce oxides at the surface in an ambient environment. The resistivity of nickel is $7 \cdot 10^{-8}$ Ωm,[140] the resistivity is six orders of magnitude larger for NiO ($2.7 \cdot 10^{-2}$ Ωm).[141] This could be one of the explanations to why it is not possible to measure any current through a reference wire made of nickel. Worth noting is that the NPs attached on-top of the electrodes in fig. 3.12, will not affect the measurement of any particle sitting in the gap, however they might effect the dimers by attracting them to other areas instead of

the nanogaps. It should be noted that the gaps seen in fig. 3.12 is designed for single particles, due to the overlapping contact arms.

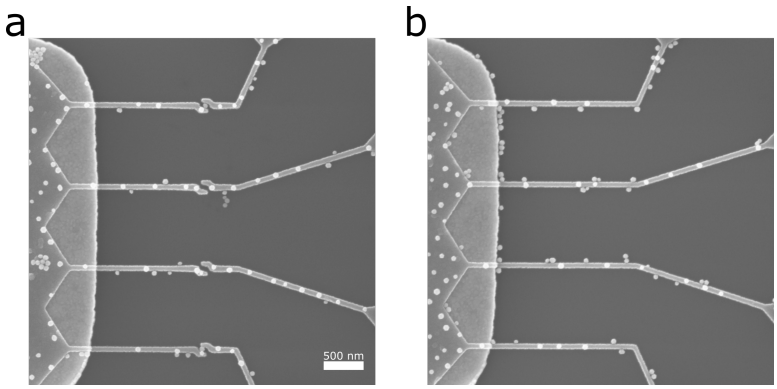

Figure 3.12: *a, Section of an array, where four out of 60 electrode pairs is seen. The sample consists of 70 nm thick nickel on a Si/SiO_2 substrate. A mixture of 1:1 dispersion:2-propanol and a deposition time of 87 h were used during the deposition. b) Shows the four references wires, present on each sample.*

Layers of palladium was incorporated into the electrodes in order to reduce the resistance in the interface between the smaller and larger electrode parts. A thin film of Pd was at first added on-top of the nickel in order to reduce the area in which nickel gets in contact with air, and therefore suppress the build of nickel oxide in the interface. This reduced the resistance through the reference wire significantly to 90 Ω. Later versions of the electrodes also included layers of Pd sandwiched into the Ni structures, as seen in fig. 3.13, (included in paper III).

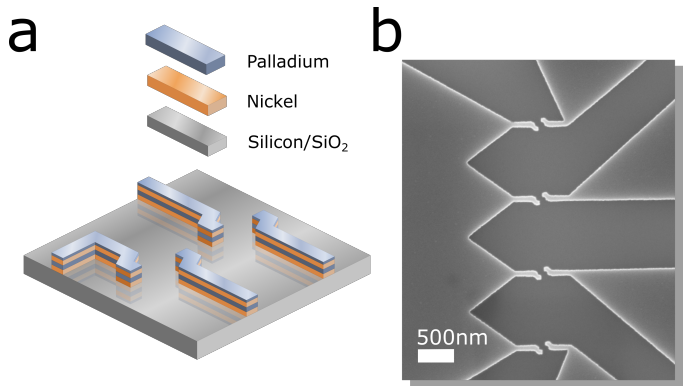

Figure 3.13: *a) Schematic overview of prefabricated nanoelectrodes, used to attract NPs. Each layer is 20 nm thick, except for the final layer of Pd at 3 nm. b) An SEM micrograph of the sandwiched electrodes. (reprinted with permission from small).*

The sandwiched electrodes consists of three layers (Ni, Pd, Ni) each with a thickness of 20 nm. A final Pd layer (3 nm thick) was added on-top of the electrodes. The idea of the layered metals is that a deposited particles should contact at least one layer of Pd inside the nanogap, hence improving the conductance measurements. The reference resistance was measured to 62 Ω, improving the conductance even further.

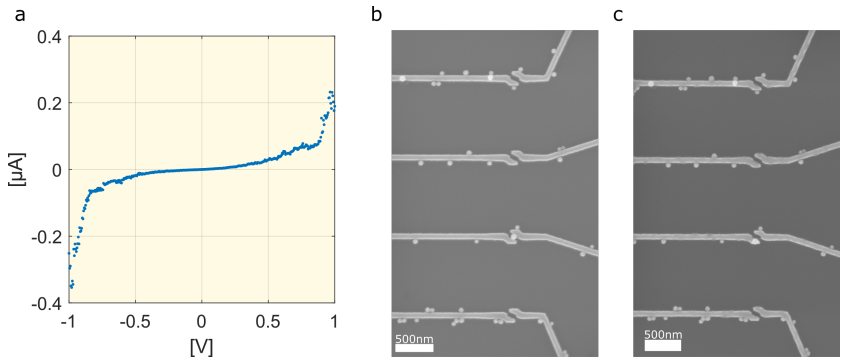

Figure 3.14: *a) Conductance measurement of a citrate stabilized single NP. b) SEM micrograph of the NP, positioned in the second to last gap counting from above. c) SEM micrograph over the same set of electrodes, b) prior to the electrical measurement and c) after the measurement. Worth noting is that the particle in b) is gone in c). The deposition took 48 h and a mixture of 1:1 dispersion:2-propanol was used.*

An I/V measurement on a single NP can be seen in fig. 3.14 a. It is the same pattern as seen in fig. 3.12, but with a 3 nm thick Pd layer on-top of the Ni and not the sandwiched electrodes as seen in fig. 3.13. The number of particles seen on-top of the electrodes, in fig. 3.14 b, have decreased compared to the electrodes in fig. 3.12. However the PSD of dimers have also decreased to 25 %, which is a drawback of the protective Pd layer. SEM micrograph after the I/V-measurement can be seen fig. 3.14 c, worth noting here is that the nanogap filled with a particle in fig. 3.14 b, is gone in c showing that particles might jump off from a nanogap. One can see from the conductance curve in fig. 3.14 a, that the measurement through a single NPs follows a non-ohmic behaviour, this might be due to tunnelling[142] from small nanogaps between the particle and the electrodes, however more experiments is needed in order to confirm this.

3.2 Self-assembly of nanoparticle dimers (paper III)

Only single NP depositions have been discussed at this point, the studies presented in the previous sections have been of great importance and have improved the deposition and made it possible to do electronic measurements on single nanoparticles. However the main goal of this thesis is to deposit and measure molecules linked between two NPs, this section will therefore treat the formation and deposition of such onto prefabricated nanosized structures.

Two molecules, benzene 1,4-dithiol (BDT) and 1,6-hexanedithiol (HDT) have been used in the studies that is presented in paper III. The resistance for BDT was measured by Xiao et al.[25] to 1.2 MΩ and for HDT (measured by Nishikawa et al.[65]) to a minimum of 614.6 MΩ. It is therefore a clear difference in resistance for the single molecules placed between the two particles. We wanted to see if it was possible to detect the same difference in resistance between the two particles. Dimers linked with the corresponding molecules were therefore formed by mixing NPs with the molecules mentioned above. TEM (transmission electron microscope) shows (fig. 3.15) that 24 % dimers exists in the colloidal dispersion after the addition of BDT and 21 % dimers could be found after the addition of HDT (The dimer synthesis and TEM measurements were performed by Tina Gschneidtner).

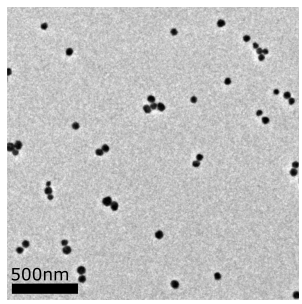

Figure 3.15: *TEM (transmission electron microscope) micrograph of dimer NP linked with BDT.*

SEM micrographs of three sets of nanogaps, with the same design as the electrodes in fig. 3.13, can be seen in can be seen in fig. 3.16. BDT linked dimers were deposited on fig. 3.16 a and b, and HDT linked dimers on c. It should be noted that a and b are from the same sample. All three sets of electrodes have a dimer attached in the nanogap. It is however only the dimer in a and c which are going to conduct, the dimer in b is only attached to one of the electrodes. This reduces the probability of attaching functional dimers to a gap significantly, the PSD of dimers are low for both BDT and HDT linked dimers, 5 % for c and 7 % for a. This was expected due to the low percentage of dimers (24 %) forming in the colloidal dispersion when adding BDT or HDT. The frequency of capturing single particles for nickel electrodes combined with palladium, was 25 %,

the combination of these two probabilities gives 6 %, which is the PSD of dimers in fig. 3.16. The percentage of dimers forming when adding molecule linker or the filtration of dimers[143] might therefore increase the PSD of dimers in the electrodes seen in fig. 3.13.

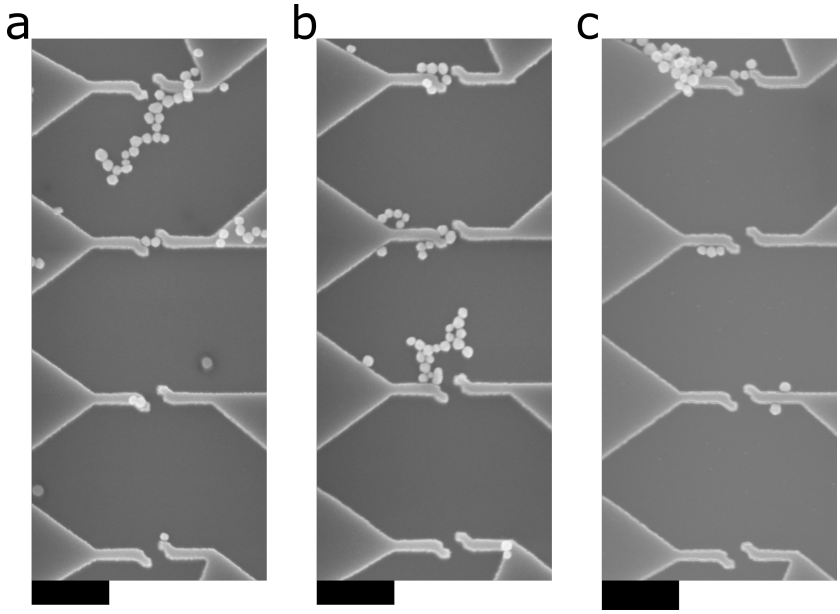

Figure 3.16: *SEM micrographs of three sets of Ni, Pd, Ni, Pd nanoelectrodes, with deposited dimers. The dimers in a) and b) are linked with BDT and c) with HDT. The scalebar in the migrographs is 500 nm. The deposition time was set to 46 h and a mixture of 1:2 dispersion:2-propanol was used for these samples.*

Electrical measurements can be seen in fig. 3.17 a, where the black solid line corresponds to an empty gap, the blue solid line to a HDT linked dimer and the red solid line to a BDT linked dimer. These measurements are only meant as a proof of concept, to shows that it is possible to conduct current through a deposited dimer. The measurements in fig. 3.17 gives only a primary indication that the resistance is lower in BDT linked dimers. One should note that more statistics is needed in order to draw stronger conclusions, which has already been made in break-junction measurements performed by others.[25,65] Extra measurements plotted in log-log scale can be seen in fig. 3.17 b, where the solids lines are the same as the one seen in a. The blue dotted lines corresponds to HDT linked dimers and the red dotted lines to BDT linked dimers. One should note that the dotted data points may also correspond to trimers. The same trend can however be seen in these plots as well, that the conductance is higher for BDT linked dimers compared to HDT linked dimers. SEM were performed on the sample prior to the electrical measurements which might affect the result.

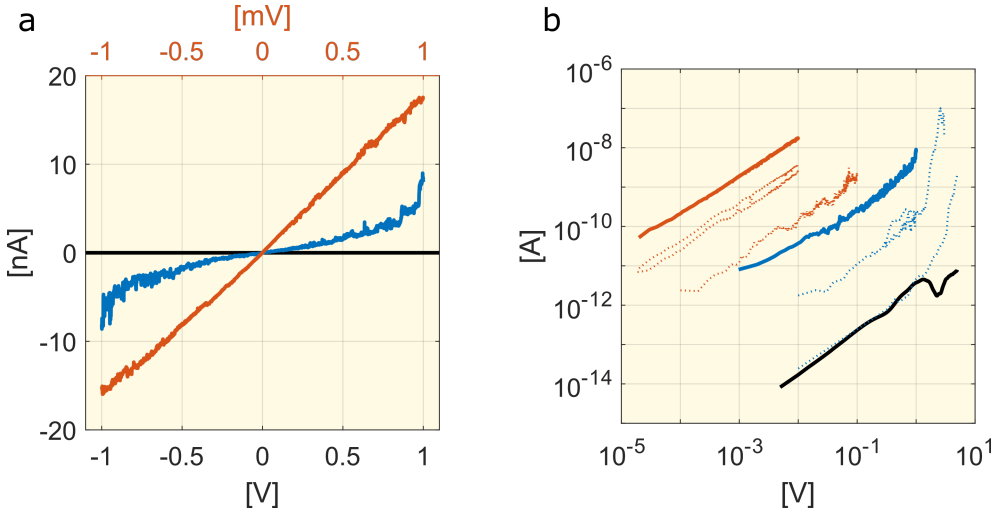

Figure 3.17: *Electrical measurements corresponding to the dimers seen in fig. 3.16. a) The red solid line corresponds to a HDT linked dimer, the blue line to a BDT linked dimer and the black line to an empty gap. The red plot is connected to the top x-axis, the rest to the bottom x-axis. b) Is a log-log plot, where the solid lines corresponds to the same lines seen in a). The dotted lines are additional measurements, some of them can also be on trimers.*

4 Concluding remarks and outlook

The increasing demand for processing power in computers have pushed the limits on how far the miniaturization of integrated electronics can continue. However, new technologies and methods are needed in order to be able to continue this trend even further. Molecular electronics seems to be an interesting option due the size range within the sub 10-nm range and the possibility to synthesis them in molar amounts. However one needs to find a way to position millions of molecules in parallel. It has been shown by other scientists that it is possible to construct nanogaps in the sub-10 nm regime using electromigration, advanced EBL, cracked-defined nanogaps, growth limited electrodes and more. It has been proven difficult to deposit single molecules in parallel using these techniques. Our approach is to first link a molecule between two NPs dimer or proto-device and then guide them towards nanoelectrode gaps optimized to attract these structures, in parallel. It is possible to deposit single molecules into nanogaps in parallel using this procedure. Pre-studies showed that the amount of deposited particles could be controlled either by a functionalized Si/SiO_2 surface (using APTES and PLL-HBr) or using other surfaces such as aluminium and nickel. This can be explained by the surface potential of materials which is negative for SiO_2 and positive for aluminium and nickel at pH 7. Citrate stabilized (negatively charged) particles are therefore attracted to nickel and repulsed by SiO_2. This is also confirmed by surface potential measurements, derived from fitting the force curve of an AFM tip approaching the surface of interest, to DLVO theory (Paper II). The deposition of NPs on a surface was described by a combination of DLVO and RSA. Inter-particle distance measurements confirmed that the deposition process is similar to the one described in theory in paper I. One should note that some parameters are assumed, such as the debye length. It is not possible for us to calculate the debye length, since the ion concentration in the solution is unknown (Sigma Aldrich do not know either). One should also keep in mind that the DLVO theory in paper I is approximated to a symmetric monovalent salt(1:1), trisodium citrate is however a salt with the valency 3:1, which might affect the results of the simulations performed in paper I.

We have in this thesis focused on linking NPs into dimers using molecules, which can be design to work as conventional components in integrated circuits. The attractive forces between nickel and tri-sodium citrate stabilized NPs have been utilized, when guiding the NPs, and molecule linked dimers to specific sites of a substrate. The structures of the electrodes were optimized in order to maximize the deposition and the addition of 2-propanol to the colloidal dispersion improved the deposition even further. The number of clusters also increased with the addition of 2-propanol, which might deposit on the electrodes and short circuit them. The drawback of nickel is that it forms oxides in ambient environment causing the contact resistances in nickel electrodes to become too high for conductance measurements. It was therefore necessary to incorporate palladium into the nickel based electrodes in order for them to conduct, this in turn lowered the percentage of successfully deposited NPs. The PSD of dimers in turns was also quite low and only 5 % of the electrodes had a dimers successfully connected to them after deposition. This number need to be increased in order for molecular electronics to compete

with other techniques such as ultra UV lithography which will be able to write in sizes well below 10 nm.[23]

The strong repulsive forces between the Si/SiO_2 and the NPs might be the reason why 2-propanol needs to be added in order to increase the PSD of NPs. It would therefore be interesting to move from Si/SiO_2 substrates to other alternatives, which do not repulse the particles. A suggestion could be to use a lipid-bilayer as Gschneidtner et al. did.[137] Other ideas could be to use silicon carbide, with an IEP of 4.9[144] a bit higher compared to the IEP of SiO_2 of 3.9 (see table 2.2) which should make silicon carbide a bit less repulsive towards citrate stabilized NPs.

Finally let's return to the research questions in the beginning of the thesis; Is it possible to contact particles and molecular linked particles in a parallel fashion onto prefabricated nanogaps in such a way that this method can compete with conventional semiconductor based integrated circuits?

Answer; We have proven that it is possible to link a molecule between two nanoparticles and position them onto nanogaps. On the other hand, the number of functional dimers positioned in the nanogaps is still too low in order to compete with conventional semiconductor industry. It is clear that one explanation is the low percentage of dimers present in the dispersion after the addition of linking molecules. A way of improving the PSD would be to separate the dimers from single particles and larger multimers, either by gel electrophoresis or filtration. Another option that might improve the PSD, could be to use a neutral charged substrate instead of the negatively charged SiO_2, such as HfO_2 with an IEP of 7.[145] This should in theory reduce the repulsive forces from the substrate and therefore increase the deposition.

Is it possible to electrically measure current through a molecule linked between two NPs deposited in a way described above, see fig. 1.3?

Answer; Yes is is possible to first link a molecule with two particles, position it between two electrodes and measure electric current through the molecule.

Will the resistance of these measurements correspond to the resistance measured by others using e.g. the break-junction technique?

Answer; The resistance through a molecule designed to work in electronics is typically in the MΩ range. Which is indeed what we measure in our experiments. We also know from the reference measurements that the prefabricated electrodes will not interfere with the measurements. However we can still se a difference in our experiments compared to break-junction measurements performed by others. The reason for this might be due to the fact that several molecules can link the dimers.

Bibliography

[1] T. C. Kriss and V. M. Kriss, "History of the operating microscope: From magnifying glass to microneurosurgery," *Neurosurgery*, vol. 42, no. 4, pp. 899–907, 1998.

[2] E. W. Pugh and L. Heide, "Early Punched Card EQUIPMENT: 1880–1951," *Proceedings of the IEEE*, vol. 101, no. 2, pp. 546–552, 2013.

[3] J. Rao, *History of Rotating Machinery Dynamics*. Via Di Biasio 43, 03043 Cassino (Fr), Italy: Springer, 2011.

[4] T. Haigh, M. Priestley, and C. Rope, *ENIAC in action : making and remaking the modern computer*. Cambridge, Massachusetts, USA: The MIT Press, 2016.

[5] W. B. Fritz, "ENIAC-a problem solver," *IEEE Annals of the History of Computing*, vol. 16, no. 1, pp. 25–45, 1994.

[6] M. Riordan, L. Hoddeson, and C. Herring, "The invetion of the transistor," *Reviews of Moders Physics*, vol. 71, no. 2, pp. S336–S345, 1999.

[7] F. Hüning, *The Fundamentals of Electrical Engineering for Mechatronics*. Rosenheimer Straße 143, 81671 München, Germany: De Gruyter, 2014.

[8] T. R. Kuphaldt, "Tubes versus semiconductor." `https://www.allaboutcircuits.com/textbook/semiconductors/chpt-13/tubes-versus-semiconductors/`. Accessed: 2018-08-17.

[9] I. W. Stats, "Internet growth statistics." `https://www.internetworldstats.com/emarketing.htm`. Accessed: 2018-08-17.

[10] I. T. Union, "Total internet users." `https://www.itu.int/en/ITU-D/Statistics/Pages/stat/default.aspx`. Accessed: 2018-08-17.

[11] "Advancing moores law in 2014: The road to 14 nm." `http://www.intel.se/content/www/se/sv/silicon-innovations/advancing-moores-law-in-2014-presentation.html`. Accessed: 2016-11-01.

[12] statista, "Internet of things (iot) connected devices installed base worldwide from 2015 to 2025 (in billions)." `https://www.statista.com/statistics/471264/iot-number-of-connected-devices-worldwide/`. Accessed: 2018-08-17.

[13] T. Ito and S. Okazaki, "Pushing the limits of lithography," *Nature*, vol. 406, pp. 1027–1031, 2000.

[14] X. Shi and S. A. Boden, "Chapter 17 - scanning helium ion beam lithography," in *Materials and Processes for Next Generation Lithography* (A. Robinson and R. Lawson, eds.), vol. 11 of *Frontiers of Nanoscience*, pp. 563 – 594, Elsevier, 2016.

[15] F. Cerrina and G. Grenci, "X-ray lithography," in *Reference Module in Materials Science and Materials Engineering*, Elsevier, 2016.

[16] S. M. Sze, *Semiconductor Devices Physics and Technology*. River Street, Hoboken, NJ 07030, USA: John Wiley & Sons, Inc, 2 ed., 2002.

[17] J. Dong, J. Liu, G. Kang, J. Xie, and Y. Wang, "Pushing the resolution of photolithography down to 15nm by surface plasmon interference," *Scientific reports*, vol. 4, p. 5618, 2014.

[18] L. R. Harriott, "Limits of lithography," *Proceedings of the IEEE*, vol. 89, no. 3, pp. 366–374, 2001.

[19] Intel, "14 nm transistor explained following the path of moore's law." `https://www.intel.sg/content/www/xa/en/silicon-innovations/standards-14nm-explained-video.html`. Accessed: 2018-10-30.

[20] M. Rommel, B. Nilsson, P. Jedrasik, V. Bonanni, A. Dmitriev, and J. Weis, "Sub-10nm resolution after lift-off using hsq/pmma double layer resist," *Microelectronic Engineering*, vol. 110, pp. 123 – 125, 2013.

[21] M. Lapedus, "What happened to nanoimprint litho?." `https://semiengineering.com/what-happened-to-nanoimprint-litho/`, March 2018. Accessed: 2018-08-20.

[22] B. Wu and A. Kumar, "Extreme ultraviolet lithography: A review," *Journal of Vacuum Science & Technology B: Microelectronics and Nanometer Structures Processing, Measurement, and Phenomena*, vol. 25, no. 6, pp. 1743–1761, 2007.

[23] S. K. Moore, "Euv lithography finally ready for chip manufacturing." `https://spectrum.ieee.org/semiconductors/nanotechnology/euv-lithography-finally-ready-for-chip-manufacturing`, January 2018. Accessed: 2018-08-20.

[24] B. E. Tebikachew, H. B. Li, A. Pirrotta, K. Börjesson, G. C. Solomon, J. Hihath, and K. Moth-Poulsen, "Effect of ring strain on the charge transport of a robust norbornadiene-quadricyclane-based molecular photoswitch," *The Journal of Physical Chemistry C*, vol. 121, no. 13, pp. 7094–7100, 2017.

[25] X. Xiao, B. Xu, and N. Tao, "Measurement of single molecule conductance: Benzenedithiol and benzenedimethanethiol," *Nano Letters*, vol. 4, no. 2, pp. 267–271, 2004.

[26] D. K. James and J. M. Tour, *Molecular Wires*, pp. 33–62. Berlin, Heidelberg: Springer Berlin Heidelberg, 2005.

[27] S. Y. Quek, M. Kamenetska, M. L. Steigerwald, H. J. Choi, S. G. Louie, M. S. Hybertsen, J. B. Neaton, and L. Venkataraman, "Mechanically controlled binary conductance switching of a single-molecule junction.," *Nature nanotechnology*, vol. 4, pp. 230–234, 2009.

[28] X. Li, J. Hihath, F. Chen, T. Masuda, L. Zang, and N. Tao, "Thermally activated electron transport in single redox molecules," *Journal of the American Chemical Society*, vol. 129, pp. 11535–11542, 2007.

[29] N. J. Tao, "Probing Potential-Tuned Resonant Tunneling through Redox Molecules with Scanning Tunneling Microscopy," *Physical Review Letters*, vol. 76, no. 21, pp. 4066–4069, 1996.

[30] K. Moth-Poulsen, ed., *Handbook of Single-Molecule Electronics*. 6000 Broken Sound Parkway NW, Suite 300 Boca Raton, FL 33487-2742: CRC Press Taylor & Francis Group, 2015.

[31] A. Aviram and M. A. Ratner, "Molecular rectifiers," *Chemical Physics Letters*, vol. 29, no. 2, pp. 277–283, 1974.

[32] I. Díez-Pérez, J. Hihath, Y. Lee, L. Yu, L. Adamska, M. A. Kozhushner, I. I. Oleynik, and N. Tao, "Rectification and stability of a single molecular diode with controlled orientation.," *Nature chemistry*, vol. 1, pp. 635–41, 2009.

[33] E. Lörtscher, B. Gotsmann, Y. Lee, L. Yu, C. Rattner, and H. Riel, "Transport Properties of a Single-Molecule Diode," *ACS nano*, vol. 6, no. 6, pp. 4931–4939, 2012.

[34] B. Capozzi, J. Xia, O. Adak, E. J. Dell, Z.-F. Liu, J. C. Taylor, J. B. Neaton, L. M. Campos, and L. Venkataraman, "Single-molecule diodes with high rectification ratios through environmental control," *Nature Nanotechnology*, vol. 10, pp. 522–527, 2015.

[35] D. Xiang, H. Jeong, T. Lee, and D. Mayer, "Mechanically controllable break junctions for molecular electronics," *Advanced Materials*, vol. 25, no. 35, pp. 4845–4867, 2013.

[36] M. A. Reed, C. Zhou, C. J. Muller, T. P. Burgin, and J. M. Tour, "Conductance of a molecular junction," *Science*, vol. 278, pp. 252–254, 1997.

[37] M. Kiguchi and S. Kaneko, "Single molecule bridging between metal electrodes," *Phys. Chem. Chem. Phys.*, vol. 15, no. 7, pp. 2253–2267, 2013.

[38] N. Muthusubramanian, E. Galan, C. Maity, R. Eelkema, F. C. Grozema, and H. S. J. van der Zant, "Insulator-protected mechanically controlled break junctions for measuring single-molecule conductance in aqueous environments," *Applied Physics Letters*, vol. 109, no. 1, p. 013102, 2016.

[39] C. Li, I. Pobelov, T. Wandlowski, A. Bagrets, A. Arnold, and F. Evers, "Charge transport in single au — alkanedithiol — au junctions: Coordination geometries and conformational degrees of freedom," *Journal of the American Chemical Society*, vol. 130, no. 1, pp. 318–326, 2008.

[40] G.Binnig and C. F. Quate, "Atomic force microscope," *Physical Review Letters*, vol. 56, pp. 930–933, 1986.

[41] Z. Li, M. Smeu, S. Afsari, Y. Xing, M. A. Ratner, and E. Borguet, "Single-molecule sensing of environmental pH - An STM break junction and NEGF-DFT approach," *Angewandte Chemie - International Edition*, vol. 53, pp. 1098–1102, 2014.

[42] X. Hao, N. Zhu, T. Gschneidtner, E. Ö. Jonsson, J. Zhang, K. Moth-Poulsen, H. Wang, K. S. Thygesen, K. W. Jacobsen, J. Ulstrup, and Q. Chi, "Direct measurement and modulation of single-molecule coordinative bonding forces in a transition metal complex," *Nature communications*, vol. 4, no. July, p. 2121, 2013.

[43] T. Dadosh, Y. Gordin, R. Krahne, I. Khivrich, D. Mahalu, V. Frydman, J. Sperling, A. Yacoby, and I. Bar-Joseph, "Measurement of the conductance of single conjugated molecules.," *Nature*, vol. 436, pp. 677–680, 2005.

[44] A. Guttman, D. Mahalu, J. Sperling, E. Cohen-Hoshen, and I. Bar-Joseph, "Self-assembly of metallic double-dot single-electron device," *Applied Physics Letters*, vol. 99, pp. 063113–1, 2011.

[45] L. A. Bumm, J. J. Arnold, M. T. Cygan, T. D. Dunbar, T. P. Burgin, L. J. Ii, D. L. Allara, J. M. Tour, and P. S. Weiss, "Are Single Molecular Wires Conducting?," *Science*, vol. 271, pp. 1705–1707, 1996.

[46] J. M. Baik, S. J. Lee, and M. Moskovits, "Polarized surface-enhanced raman spectroscopy from molecules adsorbed in nano-gaps produced by electromigration in silver nanowires," *Nano Letters*, vol. 9, no. 2, pp. 672–676, 2009. PMID: 19159247.

[47] H. S. J. van der Zant, E. A. Osorio, M. Poot, and K. O. Kavli, "Electromigrated molecular junctions," *physica status solidi (b)*, vol. 243, no. 13, pp. 3408–3412, 2006.

[48] H. B. Heersche, G. Lientschnig, K. O'Neill, H. S. J. van der Zant, and H. W. Zandbergen, "In situ imaging of electromigration-induced nanogap formation by transmission electron microscopy," *Applied Physics Letters*, vol. 91, no. 7, p. 072107, 2007.

[49] H. Park, A. Lim, A. Alivisatos, J. Park, and P. McEuen, "Fabrication of metallic electrodes with nanometer separation by electromigration," *Applied Physics Letters*, vol. 75, no. 1999, pp. 301–303, 1999.

[50] V. M. Serdio V, T. Muraki, S. Takeshita, D. E. Hurtado S, S. Kano, T. Teranishi, and Y. Majima, "Gap separation-controlled nanogap electrodes by molecular ruler electroless gold plating," *RSC Adv.*, vol. 5, pp. 22160–22167, 2015.

[51] S. Kubatkin, A. Danilov, M. Hjort, Jérôme, Cornil, J.-L. Brédas, N. Stuhr-Hansen, P. Hedegård, and T. Bjørnholm, "Single-electron transistor of a single organic molecule with access to several redox states," *Nature*, vol. 425, pp. 698–701, 2003.

[52] M. Kölbel, R. W. Tjerkstra, J. Brugger, C. J. M. Van Rijn, W. Nijdam, J. Huskens, and D. N. Reinhoudt, "Shadow-Mask Evaporation through Monolayer-Modified Nanostencils," *Nano Letters*, vol. 2, no. 12, pp. 1339–1343, 2002.

[53] L. Jiang, H. Dong, Q. Meng, J. Tan, W. Jiang, C. Xu, Z. Wang, and W. Hu, "Molecular crystal lithography: A facile and low-cost approach to fabricate nanogap electrodes," *Advanced Materials*, vol. 24, no. 5, pp. 694–698, 2012.

[54] T. Jain, S. Lara-Avila, Y. V. Kervennic, K. Moth-Poulsen, K. Nørgaard, S. Kubatkin, and T. Bjørnholm, "Aligned growth of gold nanorods in PMMA channels: Parallel preparation of nanogaps," *ACS Nano*, vol. 6, no. 5, pp. 3861–3867, 2012.

[55] Y. Majima, G. Hackenberger, Y. Azuma, S. Kano, K. Matsuzaki, T. Susaki, M. Sakamoto, and T. Teranishi, "Three-input gate logic circuits on chemically assembled single-electron transistors with organic and inorganic hybrid passivation layers," *Science and Technology of Advanced Materials*, vol. 18, no. 1, pp. 374–380, 2017.

[56] V. Dubois, F. Niklaus, and G. Stemme, "Crack-Defined Electronic Nanogaps," *Advanced Materials*, vol. 28, pp. 2178–2182, 2016.

[57] C. Jia, A. Migliore, N. Xin, S. Huang, J. Wang, Q. Yang, S. Wang, H. Chen, D. Wang, B. Feng, Z. Liu, G. Zhang, D.-H. Qu, H. Tian, M. A. Ratner, H. Q. Xu, A. Nitzan, and X. Guo, "Covalently bonded single-molecule junctions with stable and reversible photoswitched conductivity," *Science*, vol. 352, no. 6292, pp. 1443–1445, 2016.

[58] Y. D. Fernandez, L. Sun, T. Gschneidtner, and K. Moth-Poulsen, "Research update: Progress in synthesis of nanoparticle dimers by self-assembly," *APL Materials*, vol. 2, no. 1, p. 010702, 2014.

[59] T. A. Gschneidtner, Y. A. Diaz Fernandez, and K. Moth-Poulsen, "Progress in self-assembled single-molecule electronic devices," *Journal of Materials Chemistry C*, vol. 1, pp. 7127–7133, 2013.

[60] M. Dewi, T. Gschneidtner, S. Elmas, M. Ranford, K. Moth-Poulsen, and T. Nann, "Monofunctionalization and dimerization of nanoparticles using coordination chemistry," *ACS Nano*, vol. 9, no. 2, pp. 1434–1439, 2015. PMID: 25494037.

[61] T. Jain, Q. Tang, T. Bjørnholm, and K. Nørgaard, "Wet chemical synthesis of soluble gold nanogaps," *Accounts of Chemical Research*, vol. 47, no. 1, pp. 2–11, 2014.

[62] S. Kano, K. Maeda, D. Tanaka, M. Sakamoto, T. Teranishi, and Y. Majima, "Chemically assembled double-dot single-electron transistor analyzed by the orthodox model considering offset charge," *Journal of Applied Physics*, vol. 118, no. 13, p. 134304, 2015.

[63] K. S. Makarenko, Z. Liu, M. P. de Jong, F. A. Zwanenburg, J. Huskens, and W. G. van der Wiel, "Bottom-up single-electron transistors," *Advanced Materials*, vol. 29, no. 42, p. 1702920, 2017.

[64] A. Ulfkjær, F. W. Nielsen, H. Al-Kerdi, T. Ruß, Z. K. Nielsen, J. Ulstrup, L. Sun, K. Moth-Poulsen, J. Zhang, and M. Pittelkow, "A gold-nanoparticle stoppered [2]rotaxane," *Nanoscale*, vol. 10, pp. 9133–9140, 2018.

[65] A. Nishikawa, J. Tobita, Y. Kato, S. Fujii, M. Suzuki, and M. Fujihira, "Accurate determination of multiple sets of single molecular conductance of au/1,6-hexanedithiol/au break junctions by ultra-high vacuum-scanning tunneling microscope and analyses of individual current-separation curves," *Nanotechnology*, vol. 18, no. 42, p. 424005, 2007.

[66] M. Kumar, "Molecular diodes and applications," *Recent Patents on Nanotechnology*, vol. 1, pp. 51–57, 2007.

[67] "Pn junction diode." `https://www.electronics-tutorials.ws/diode/diode3.html`. Accessed: 2018-09-07.

[68] N. J. Geddes, J. R. Sambles, D. J. Jarvis, W. G. Parker, and D. J. Sandman, "Fabrication and investigation of asymmetric currentvoltage characteristics of a metallangmuirblodgett monolayermetal structure," *Applied Physics Letters*, vol. 56, no. 19, pp. 1916–1918, 1990.

[69] N. J. Geddes, J. R. Sambles, D. J. Jarvis, W. G. Parker, and D. J. Sandman, "The electrical properties of metal-sandwiched langmuir-blodgett multilayers and monolayers of a redox-active organic molecular compound," *Journal of Applied Physics*, vol. 71, no. 2, pp. 756–768, 1992.

[70] R. M. Metzger, "Electrical rectification by a molecule: The advent of unimolecular electronic devices," *Accounts of Chemical Research*, vol. 32, no. 11, pp. 950–957, 1999.

[71] K. Moth-Poulsen, D. Ćoso, K. Börjesson, N. Vinokurov, S. K. Meier, A. Majumdar, K. P. C. Vollhardt, and R. A. Segalman, "Molecular solar thermal (MOST) energy storage and release system," *Energy & Environmental Science*, vol. 5, pp. 8534–8537, 2012.

[72] F. Chen, X. Li, J. Hihath, Z. Huang, and N. Tao, "Effect of anchoring groups on single-molecule conductance: Comparative study of thiol-, amine-, and carboxylic-acid-terminated molecules," *Journal of the American Chemical Society*, vol. 128, pp. 15874–15881, 2006.

[73] Y. Kim, T. J. Hellmuth, D. Sysoiev, F. Pauly, T. Pietsch, J. Wolf, A. Erbe, T. Huhn, U. Groth, U. E. Steiner, and E. Scheer, "Charge transport characteristics of diarylethene photoswitching single-molecule junctions," *Nano Letters*, vol. 12, pp. 3736–3742, 2012.

[74] C. A. Martin, D. Ding, J. K. Sørensen, T. Bjørnholm, J. M. van Ruitenbeek, and H. S. J. van der Zant, "Fullerene - based anchoring groups for molecular electronics," *Journal of the American Chemical Society*, vol. 130, pp. 13198–13199, 2008.

[75] H. Häkkinen, "The gold–sulfur interface at the nanoscale," *Nature Chemistry*, vol. 4, pp. 443–455, 2012.

[76] Y. Komoto, S. Fujii, H. Nakamura, T. Tada, N. Tomoaki, and M. Kiguchi, "Resolving metal-molecule interfaces at single-molecule junctions," *Scientific Reports*, vol. 6, p. 26606, 2016.

[77] R. Courtland, "Intel now packs 100 million transistors in each square millimeter." `https://spectrum.ieee.org/nanoclast/semiconductors/processors/intel-now-packs-100-million-transistors-in-each-square-millimeter`, mars 2017. Accessed: 2018-09-10.

[78] T. Gschneidtner, Y. Fernandez, S. Syrenova, F. Westerlund, C. Langhammer, and K. Moth-Poulsen, "A versatile self-assembly strategy for the synthesis of shape-selected colloidal noble metal nanoparticle heterodimers," *Langmuir*, vol. 30, no. 11, pp. 3041–3050, 2014.

[79] C. J. Loweth, W. B. Caldwell, X. Peng, A. P. Alivisatos, and P. G. Schultz, "Dna-based assembly of gold nanocrystals," *Angewandte Chemie International Edition*, vol. 38, no. 12, pp. 1808–1812, 1999.

[80] D. Zanchet, C. M. Micheel, W. J. Parak, D. Gerion, S. C. Williams, and A. P. Alivisatos, "Electrophoretic and structural studies of dna-directed au nanoparticle groupings," *The Journal of Physical Chemistry B*, vol. 106, no. 45, pp. 11758–11763, 2002.

[81] T. Jain, F. Westerlund, E. Johnson, K. Moth-Poulsen, and T. Bjørnholm, "Self-assembled nanogaps via seed-mediated growth of end-to-end linked gold nanorods," *ACS Nano*, vol. 3, no. 4, pp. 828–834, 2009.

[82] C. Kuemin, L. Nowack, L. Bozano, N. D. Spencer, and H. Wolf, "Oriented assembly of gold nanorods on the single-particle level," *Advanced Functional Materials*, vol. 22, no. 4, pp. 702–708, 2012.

[83] S. Ni, M. J. K. Klein, N. D. Spencer, and H. Wolf, "Cascaded assembly of complex multiparticle patterns," *Langmuir*, vol. 30, pp. 90–95, 2014.

[84] J. Israelachvili, *Intermolecular and Surface Forces*. 225 Wyman Street, Waltham, MA 02451, USA: Academic Press, 3 ed., 2011.

[85] A. Rényi, "On a one-dimensional problem concerning random space filling," *Publications of the mathematical institute of the hungarian academy of sciences*, vol. 3, 1958.

[86] B. D. Ripley, "The second-order analysis of stationary point processes," *Journal of Applied Probability*, vol. 13, no. 2, pp. 255–266, 1976.

[87] M. Kiskowski, J. Hancock, and A. Kenworthy, "On the use of ripley's k-function and its derivatives to analyze domain size," *Biophysical journal*, vol. 97, pp. 1095–11003, 2009.

[88] P. Diggle, *Statistical Analysis of Spatial and Spatio-Temporal Point Patterns*, vol. 3. 6000 Broken Sound Parkway NW, Suite 300, Boca Raton, FL 33487-2742: CRC Press Taylor & Francis Group, 2014.

[89] W. Meulebroeck, H. Wouters, K. Nys, and H. Thienpont, "Authenticity screening of stained glass windows using optical spectroscopy," *Scientific Reports*, vol. 6, p. 37726, 2016.

[90] D. Barchiesi, "Lycurgus cup: inverse problem using photographs for characterization of matter," *J. Opt. Soc. Am. A*, vol. 32, pp. 1544–1555, Aug 2015.

[91] B. Gulson, M. McCall, M. Korsch, L. Gomez, P. Casey, Y. Oytam, A. Taylor, M. McCulloch, J. Trotter, L. Kinsley, and G. Greenoak, "Small amounts of zinc from zinc oxide particles in sunscreens applied outdoors are absorbed through human skin," *Toxicological Sciences*, vol. 118, no. 1, pp. 140–149, 2010.

[92] R. B. Reed, T. Zaikova, A. Barber, M. Simonich, R. Lankone, M. Marco, K. Hristovski, P. Herckes, L. Passantino, D. H. Fairbrother, R. Tanguay, J. F. Ranville, J. E. Hutchison, and P. K. Westerhoff, "Potential environmental impacts and antimicrobial efficacy of silver- and nanosilver-containing textiles," *Environmental Science & Technology*, vol. 50, no. 7, pp. 4018–4026, 2016.

[93] J. Borglin, S. Guldbrand, H. Evenbratt, V. Kirejev, H. Grönbeck, and M. B. Ericson, "Insights on proximity effect and multiphoton induced luminescence from gold nanospheres in far field optical microscopy," *Applied Physics Letters*, vol. 107, no. 23, p. 234101, 2015.

[94] A. Lundgren, M. Hulander, J. Brorsson, M. Hermansson, H. Elwing, O. Andersson, B. Liedberg, and M. Berglin, "Gold-nanoparticle-assisted self-assembly of chemical gradients with tunable sub-50 nm molecular domains," *Particle & Particle Systems Characterization*, vol. 31, no. 2, pp. 209–218, 2014.

[95] T. A. Gschneidtner, Y. A. D. Fernandez, S. Syrenova, F. Westerlund, C. Langhammer, and K. Moth-Poulsen, "A versatile self-assembly strategy for the synthesis of shape-selected colloidal noble metal nanoparticle heterodimers," *Langmuir*, vol. 30, no. 11, pp. 3041–3050, 2014.

[96] O. Bitton, D. Gutman, R. Berkovits, and A. Frydman, "Multiple periodicity in a nanoparticle-based single-electron transistor," *Nature Communications*, vol. 8, p. 402, 2017.

[97] S. Khondaker, K. Luo, and Z. Yao, "The fabrication of single-electron transistors using dielectrophoretic trapping of individual gold nanoparticles," *Nanotechnology*, vol. 21, no. 9, p. 095204, 2010.

[98] A. S. Blum, C. M. Soto, C. D. Wilson, T. L. Brower, S. K. Pollack, T. L. Schull, A. Chatterji, T. Lin, J. E. Johnson, C. Amsinck, P. Franzon, R. Shashidhar, and B. R. Ratna, "An engineered virus as a scaffold for three-dimensional self-assembly on the nanoscale," *Small*, vol. 1, no. 7, pp. 702–706, 2005.

[99] J. Byrne and J. a. Baugh, "The significance of nanoparticles in particle-induced pulmonary fibrosis," *McGill Journal of Medicine*, vol. 11, no. 1, pp. 43–50, 2008.

[100] B. Meuller, M. Messing, D. Engberg, A. Jansson, L. Johansson, S. Norlén, N. Tureson, and K. Deppert, "Review of spark discharge generators for production of nanoparticle aerosols," *Aerosol Science and Technology*, vol. 46, no. 11, pp. 1256–1270, 2012.

[101] F. Schulz, T. Homolka, N. G. Bastús, V. Puntes, H. Weller, and T. Vossmeyer, "Little adjustments significantly improve the turkevich synthesis of gold nanoparticles," *Langmuir*, vol. 30, no. 35, pp. 10779–10784, 2014.

[102] G. H. Woehrle, L. O. Brown, and J. E. Hutchison, "Thiol-functionalized, 1.5-nm gold nanoparticles through ligand exchange reactions: Scope and mechanism of ligand exchange," *Journal of the American Chemical Society*, vol. 127, no. 7, pp. 2172–2183, 2005.

[103] K. Moth-Poulsen, ed., *Handbook of Single-Molecule Electronics*. New York: Pan Stanford Publishing, 2016.

[104] R. Grubbs, "Roles of polymer ligands in nanoparticle stabilization," *Polymer Reviews*, vol. 47, no. 2, pp. 197–215, 2007.

[105] S. A. AL-Thabaiti, F. Al-Nowaiser, A. Obaid, A. Al-Youbi, and Z. Khan, "Formation and characterization of surfactant stabilized silver nanoparticles: A kinetic study," *Colloids and Surfaces B: Biointerfaces*, vol. 67, no. 2, pp. 230 – 237, 2008.

[106] T. Gschneidtner, *Building Blocks for the Assembly of Nanostructures*. PhD thesis, Chalmers University of Technology, 2017.

[107] I. Chakraborty, P. K. Malik, and S. P. Moulik, "Preparation and characterisation of cos2 nanomaterial in aqueous cationic surfactant medium of cetyltrimethylammonium bromide (ctab)," *Journal of Nanoparticle Research*, vol. 8, pp. 889–897, Dec 2006.

[108] S. Kittler, S. Hickey, T. Wolff, and A. Eychmüller, "Easy and fast phase transfer of ctab stabilised gold nanoparticles from water to organic phase," *Zeitschrift für Physikalische Chemie*, vol. 229, pp. 235–245, 2015.

[109] A. Kameo, A. Suzuki, K. Torigoe, and K. Esumi, "Fiber-like gold particles prepared in cationic micelles by uv irradiation: Effect of alkyl chain length of cationic surfactant on particle size," *Journal of Colloid and Interface Science*, vol. 241, no. 1, pp. 289 – 292, 2001.

[110] N. G. Bastús, F. Merkoçi, J. Piella, and V. Puntes, "Synthesis of highly monodisperse citrate-stabilized silver nanoparticles of up to 200 nm: Kinetic control and catalytic properties," *Chemistry of Materials*, vol. 26, no. 9, pp. 2836–2846, 2014.

[111] P. Zhao, N. Li, and D. Astruc, "State of the art in gold nanoparticle synthesis," *Coordination Chemistry Reviews*, vol. 257, no. 3, pp. 638 – 665, 2013.

[112] D. Evans and H. Wennerström, *The Colloidal Domain Where Physics, Chemistry and Technology meet.* 111 River Street, Hoboken, NJ 07030, (201) 748-6011: Wiley-VCH, 2 ed., 1999.

[113] M. Fatehah, H. Aziz, and S. Stoll, "Nanoparticle properties, behavior, fate in aquatic systems and characterization methods," *Journal of Colloid Science and Biotechnology*, vol. 3, pp. 1–30, 2014.

[114] "Malvern panalyrical zetasizer nano range." `https://www.malvernpanalytical.com/en/products/product-range/zetasizer-range/zetasizer-nano-range?gclid=EAIaIQobChMItKe694zJ3QIVTIuyCh3kjgVjEAAYASAAEgIkpfD_BwE`. Accessed: 2018-08-17.

[115] Z. Adamczyk, B. Siwek, M. Zembala, and P. Belouschek, "Kinetics of localized adsorption of colloid particles," *Advances in Colloid and Interface Science*, vol. 48, pp. 151 – 280, 1994.

[116] M. R. Oberholzer, J. M. Stankovich, S. L. Carnie, D. Y. Chan, and A. M. Lenhoff, "2-d and 3-d interactions in random sequential adsorption of charged particles," *Journal of Colloid and Interface Science*, vol. 194, no. 1, pp. 138 – 153, 1997.

[117] J. Eklöf, T. Gschneidtner, S. Lara-Avila, K. Nygård, and K. Moth-Poulsen, "Controlling deposition of nanoparticles by tuning surface charge of SiO2 by surface modifications.," *RSC Advances*, vol. 6, pp. 104246–104253, 2016.

[118] H. MAR and T. N. WIGHT, "18 - correlative light and electron microscopic immunocytochemistry on reembedded resin sections with colloidal gold," in *Colloidal Gold* (M. Hayat, ed.), pp. 357 – 378, San Diego: Academic Press, 1989.

[119] J. I. F. F. J. Gil-Llambías, A. M. Escudey and A. L. Agudo, "Determination of the active surface area of vanadia by electrophoretic migration and xps measurements," *Journal of Catalysis*, vol. 95, pp. 520–526, 1985.

[120] M. F. Cuddy, A. R. Poda, and L. N. Brantley, "Determination of isoelectric points and the role of ph for common quartz crystal microbalance sensors," *ACS Applied Materials & Interfaces*, vol. 5, no. 9, pp. 3514–3518, 2013.

[121] S. Kittaka and T. Morimoto, "Isoelectric point of metal oxides and binary metal oxides having spinel structure," *Journal of Colloid and Interface Science*, vol. 75, no. 2, pp. 398 – 403, 1980.

[122] R. Smallman and A. Ngan, *Physical Metallurgy and Advanced Materials Engineering.* Oxford: Butterworth-Heinemann, 2007.

[123] G. Celler and L. Trimble, "Formation of sio at si/sio_2 interface and its influence on transport of group v dopants and ge in sio_2," *Applied Surface Science*, vol. 39, no. 1, pp. 245 – 258, 1989.

[124] Q. Su, C. Huang, Y. Wang, Y. Fan, B. Lu, W. Lan, Y. Wang, and X. Liu, "Formation of vanadium oxides with various morphologies by chemical vapor deposition," *Journal of Alloys and Compounds*, vol. 475, no. 1?2, pp. 518 – 523, 2009.

[125] S.-K. Lee, H.-C. Hsu, and W.-H. Tuan, "Oxidation Behavior of Copper at a Temperature below 300 °C and the Methodology for Passivation," *Materials Research*, vol. 19, pp. 51 – 56, 2016.

[126] E. S. Lambers, C. N. Dykstal, J. M. Seo, J. E. Rowe, and P. H. Holloway, "Roomtemerature oxidation of ni(110) at low and atmospheric oxygen pressures," *Oxidation of Metals*, vol. 45, no. 3, pp. 301–321, 1996.

[127] W. Melitz, J. Shen, A. Kummel, and S. Lee, "Kelvin probe force microscopy and its application," *Surface Science Reports*, vol. 66, pp. 1–27, 2011.

[128] L. Collins, J. I. Kilpatrick, S. A. L. Weber, A. Tselev, I. V. Vlassiouk, I. N. Ivanov, S. Jesse, S. V. Kalinin, and B. J. Rodriguez, "Open loop kelvin probe force microscopy with single and multi-frequency excitation," *Nanotechnology*, vol. 24, no. 47, p. 475702, 2013.

[129] J. Eklöf, A. Stolaś, M. Herzberg, A. Pekkari, B. Tebikachew, T. Gschneidtner, S. Lara-Avila, T. Hassenkam, and K. Moth-Poulsen, "Guided selective deposition of nanoparticles by tuning of the surface potential," *EPL (Europhysics Letters)*, vol. 119, no. 1, p. 18004, 2017.

[130] J. Drelich, J. Long, and A. Yeung, "Determining surface potential of the bitumen-water interface at nanoscale resolution using atomic force microscopy," *The Canadian Journal of Chemical Engineering*, vol. 85, no. 5, pp. 625–634, 2007.

[131] W. Drożdż, Y. Bessin, V. Gervais, X.-Y. Cao, J.-M. Lehn, A. R. Stefankiewicz, and S. Ulrich, "Switching multivalent dna complexation using metal-controlled cationic supramolecular self-assemblies," *Chemistry - A European Journal*, vol. 24, no. 7, pp. 1518–1521, 2017.

[132] C. Ng, Y. Cheng, and P. Pennefather, "Properties of a self-assembled phospholipid membrane supported on lipobeads," *Biophysical Journal*, vol. 87, pp. 323–331, 2004.

[133] L. Nasalean, S. Baudrey, N. B. Leontis, and L. Jaeger, "Controlling rna self-assembly to form filaments," *Nucleic Acids Research*, vol. 34, no. 5, pp. 1381–1392, 2006.

[134] F. Schreiber, "Structure and growth of self-assembling monolayers," *Progress in Surface Science*, vol. 65, no. 5, pp. 151 – 257, 2000.

[135] A. Bhattacharya and B. Bansal, "26 - self-assembly in semiconductor epitaxy: From growth mechanisms to device applications," in *Handbook of Crystal Growth (Second Edition)* (T. F. Kuech, ed.), Handbook of Crystal Growth, pp. 1057 – 1099, Boston: North-Holland, second edition ed., 2015.

[136] S. Ni, J. Leemann, I. Buttinoni, L. Isa, and H. Wolf, "Programmable colloidal molecules from sequential capillarity-assisted particle assembly," *Science Advances*, vol. 2, p. e1501779, 2016.

[137] Y. A. Diaz Fernandez, T. A. Gschneidtner, C. Wadell, L. H. Fornander, S. Lara Avila, C. Langhammer, F. Westerlund, and K. Moth-Poulsen, "The conquest of middle-earth: combining top-down and bottom-up nanofabrication for constructing nanoparticle based devices.," *Nanoscale*, vol. 6, pp. 14605–14616, 2014.

[138] M. Sayin and R. Dahint, "Formation of charge-nanopatterned templates with flexible geometry via layer by layer deposition of polyelectrolytes for directed self-assembly of gold nanoparticles," *Nanotechnology*, vol. 28, p. 135303, 2017.

[139] J.-G. Park, S.-H. Lee, J.-S. Ryu, Y.-K. Hong, T.-G. Kim, and A. Busnaina, "Interfacial and electrokinetic characterization of ipa solutions related to semiconductor wafer drying and cleaning," *Journal of The Electrochemical Society*, vol. 153, pp. G811–G814, 2006.

[140] "Resistivity table / chart." `https://www.radio-electronics.com/info/formulae/resistance/resistivity-table.php`. Accessed: 2018-10-23.

[141] C. Park, J. Kim, K. Lee, O. Kun, H. Kang, and N. Park, "Electronic, optical and electrical properties of nickel oxidethin films grown by rf magnetron sputtering," *Applied Science and Convergence Technology*, vol. 24, pp. 72–76, 2015.

[142] H. Li, I. Wani, A. Hayat, S. Jafri, and K. Leifer, "Fabrication of reproducible sub-5 nm nanogaps by a focused ion beam and observation of fowler-nordheim tunneling," *Applied Physics Letters*, vol. 107, no. 10, p. 103108, 2015.

[143] M. Hanauer, S. Pierrat, I. Zins, A. Lotz, and C. Sönnichsen, "Separation of nanoparticles by gel electrophoresis according to size and shape," *Nano Letters*, vol. 7, no. 9, pp. 2881–2885, 2007.

[144] B. P. Singh, J. Jena, L. Besra, and S. Bhattacharjee, "Dispersion of nano-silicon carbide (sic) powder in aqueous suspensions," *Journal of Nanoparticle Research*, vol. 9, pp. 797–806, Oct 2007.

[145] Y. Chen, M. Liu, T. Kaneko, and M. Paul C., "Atomic layer deposited hafnium oxide gate dielectrics for charge-based biosensors," *Electrochemical and Solid-State Letters*, vol. 13, pp. G29–G32, 2010.